acta physica slovaca vol. 49 No. 5, 835 – 874 **October 1999**

HADRONIZATION AND STRANGENESS PRODUCTION IN HEAVY-ION COLLISIONS[1]

Tamás S. Biró[2], Péter Lévai, József Zimányi
MTA KFKI RMKI, Budapest P.O.Box 49, H-1525, Hungary

Christoph T. Traxler
University of Giessen, Heinrich-Buff-Ring 16, D-35392 Giessen, Germany

Received 16 December 1998, in final form 20 February 1999, accepted 22 February 1999

The hadronization process of a quark matter possibly formed in relativistic heavy ion experiments at CERN SPS and RHIC is addressed in the framework of a non-equilibrium approach using hadron formation rates for effectively massive quarks and gluons. After a brief review of the relevant thermodynamical concepts consequences of string formation on the hadron composition are investigated in the transchemical quark fusion model and in a molecular dynamical simulation of the semiclassical chromodielectric model.

PACS: 12.38Mh, 24.10Lx, 21.30Fe

1 The basic story: confinement

In the following three lectures I plan to report on our latest efforts for describing the late stage of ultrarelativistic heavy-ion collisions, especially the formation and re-hadronization of quark matter at CERN SPS energies ($\sqrt{s} \approx 20$ GeV).

In pedagogical order I shall first start with a brief review of the color confinement phenomenon in QCD and explain how we intend to incorporate it into phenomenological models. Then a review of theoretical approaches follows with an emphasis on the needs of heavy-ion physics. The first lecture is closed then by a recitation of a method known from physical chemistry, which establishes a relation between an equation of state (EOS) and the characteristic correlation length of the physical system described by that EOS.

The second lecture is basically designated to the investigations of quark matter — hadronic matter mixtures with a string-like interaction among the non-hadronic components. This concludes in the transchemistry model (TrCHEM), which describes the time-evolution of such a mixture from a hot constituent quark-matter state into a purely hadronic state. In the virtue of this model all color charges will be eliminated and the calculation ends up with ground-state and

[1]Talk held by T.S.Biró at the Workshop on Heavy-Ion Collisions, Aug 31 - Sep 4, 1998, Modra, Slovakia
[2]E-mail address: tsbiro@sunserv.kfki.hu

low-lying resonances of mesons, baryons and anti-baryons. These results will then be compared with some already available experimental data.

In the third lecture our first results stemming from a classical molecular dynamical simulation of the chromodielectric model will be reported. This work is computationally very involved, since not only the motion of extended (albeit classical) color charges but also the evolution of chromoelectric fields are calculated. The solution of the Gauss law constraint in this process requires special numerical procedures.

The most characteristic feature of confinement is that the energy of any color non-singlet state is infinite in an infinite volume:

$$\lim_{V \to \infty} E \to \infty. \tag{1}$$

This allows for the existence of color charges in a finite volume for a finite time: a general notion of quark matter. Due to the confinement, however, the equation of state of such a quark matter shows an instability (negative pressure) in the thermodynamical limit $V \to \infty$. At high enough temperature on the other hand this pressure becomes positive and ultimately oversizes the pressure of the hadronic matter. From this point the quark matter is not only stable, but the preferred equilibrium state.

The experimental quest for quark matter can be grouped into three classes of efforts seeking for measurable consequences of its production (rapidity and transverse energy distributions), lifetime (HBT) and decay products (strange mesons, multiple strange anti-baryons, lepton pairs, signals of disoriented chiral condensates). Whatsoever exciting the theoretical expectations are, heavy-ion reactions can be characterized with the following unpleasant properties:

- no equilibrium state,
- no ideal quark-gluon plasma and
- no strong signal

has been produced (yet). Ongoing heavy-ion experiments use gold (Au) and lead (Pb) beams at the AGS (Brookhaven) and SPS (CERN) synchrotrons, respectively. The achieved energy in these fixed target experiments amounts to $\sqrt{s} = 4$ and $\sqrt{s} = 17$ GeV, leaving room for theoretical expectations of a maximal temperature of $T_0 \approx 150 - 190$ MeV in a totally equilibrized state (which is an idealization).

There is a clear urge for higher energy accelerator experiments. Plans are already improved for the RHIC (at Brookhaven) with $\sqrt{s} = 200$ GeV and for the LHC (at CERN) with $\sqrt{s} = 6300$ GeV per nucleon collider energies. While in these future experiments a higher degree of energy density and temperature is expected, far in the region of quark-gluon plasma (if we shall not deal with an unexpected increase of transparency of nuclei), the already ongoing measurements seem to offer a neither hadronic nor ideal quark-gluon plasma scenario. At this point I would just like to pick up — somewhat arbitrarily — two features: i) there seems to be a strangeness enhancement in heavy-ion collisons with respect to the mere superposition of nucleon-nucleon collisions, (this occurs already at AGS, but is most expressed at SPS) and ii) there is a possibly sudden suppression of heavy charm meson production (J/ψ) as a function of the transverse energy (NA50 1997) indicating a qualitative change in the properties of the produced fireball.

1.1 Theoretical approaches to heavy-ion physics

In the followings I would like to present a brief evaluation of established and newer theoretical methods used in relativistic heavy-ion physics. I divided them into six classes, from which three of each form a larger group. The first three are methods stemming from elementary particle and field theory, while the second three have their roots rather in many particle phenomenology. In the present stage of the theory both approaches are necessary in order to gain a complementative insight into the dynamics of quark matter formation and re-hadronization.

1. **Lattice QCD** has the advantage that it is a gauge-covariant, non-perturbative approach based on the elementary fields mediating the strong interaction. It is, however, not yet perfect for purposes of the heavy-ion community due to the lack of a reliable treatment of non-equilibrium states, finite baryon charge and fast transitions without phase coexistence. The main results of this method, which are used by other — more phenomenological — approaches as well, can be summarized as follows: a qualitative understanding of heavy quark confinement and the color deconfinement phase transition; quantitaively the relation between the string tension ($\sigma_s \approx 1$ GeV/fm) and the deconfinement temperature ($T_c \approx 0.5\sqrt{\sigma_S} \approx 220$ MeV for a pure gluonic system and $T_c \approx 160$ MeV for a realistic number of light quark flavors.)

2. **perturbative QCD** is (in principle) free from numerical uncertainities and does not require an extensive computer use. It is an analytic method and — at least partially — resummable, making thus available some results, which are valid also for strong coupling. The best examples are transport properties of high temperature QCD plasma. Backdraw of this method is, that it cannot presently deal with some important non-perturbative effects, as the chromomagnetic mass, and due to its basic philosophy is restricted to near-equilibrium states (the range of linear response theory). Characteristic results of this method are transport coefficients, effective masses and screening lengthes in quark-gluon plasma.

3. **Effective field theories** were developed with the aim of simplifying QCD into a solvable, but still confining theory. Two most characteristic instances of this type are the Nambu Jona-Lasinio Model (NJL) and the Friedberg-Lee or Chromodielectric Model (CDM). The NJL model does not contain the color degree of freedom explicitely, it incorporates hadronic degrees of freedom into the model Lagrangian instead. Being deviced for the description of the chiral phase transition (and showing a close relationship to the O(4) sigma model) it succeeds in describing the mass difference between bare and effective quarks. Recently hadronization cross sections were obtained in the framework of this model. The CDM model on the other hand takes over the non-abelian gluon fields from QCD. These are then treated in the abelian approximation on the mean field level and all non-abelian effects are shuffled into the use of a phenomenological scalar field, which in turn governs the color confinement via its effect on the chromodielectric constant in the vacuum state. This model is able to provide microscopic information on the evolution of color during the re-hadronization of quark-gluon matter; bag fragmentation and string pulling can be observed in simulations. A molecular dynamical simulation of this model applied for the hadronization process of a piece of hot quark-gluon plasma was the issue of a recent work, I shall discuss it in more detail in the third lecture.

4. **Thermal models** are the simplest phenomenological models dealing with a few global parameters like temperature, baryochemical and strange potential. Here not the understanding of possible solutions to QCD by simulation is aimed at, but rather the description of experimental findings, irrespective of color dynamics, gauge symmetry or quantum effects. The most trivial backdraw of this approach is its restriction to equilibrium states and the neglection of any concept of confinement. Nevertheless practical information, like particle ratios, rapidity- and transverse momentum spectra can be obtained relatively easily in such models.

5. **Microdynamical models** (RQMD,UrQMD, QGSM, VENUS, Parton Cascade, HIJING, etc.) are typically extended numerical simulations of the time evolution of hadronic and quark content of the reaction zone in heavy-ion collisions. They deal with fairly off-equilibrium situations. Although they usually succeed in getting simulation results which are commensurate with experimental data, the excessive use of parameters makes it increasingly difficult to interpret these results in terms of elementary field concepts. The more complicated the simulation, the less can we learn about the original. It is presently also ambiguous, how to incorporate long range collective effects, in particular confinement.

6. **Chemical models** can be characterized as a compromise between thermal and microdynamical models: some selected features — mostly the particle composition — are treated dynamically and the vast of parameters only statistically. This way such models can remain relatively simple and deal with non-equilibrium phenomena. Effects of confinement can be incorporated via the use of non-ideal equations of state. By choosing the key equation of state, both quark-matter and hadronic matter assumptions can be tested on the evolution of particle ratios and predictions can be made for hadron spectra observed in heavy-ion experiments. A particular model — the transchemistry model — is based on a color confining equation of state describing constituent quark matter and its neutral clusters assuming an interaction between colored objects which is mediated by strings. It will be discussed in the second lecture.

1.2 Equation of State and Correlations

It is perhaps not widely known that an equation of state may carry information about the characteristic length of spatial correlations between the thermodynamical variables. This effect of course goes beyond the mean field approximation. A relatively simple nearest-neighbour correction, however, already leads to equations of state which include information about pair-correlation.

A well-known example is probably the hard-core effect: due to strong repulsive forces the particle never approach each other too closely, so an anti-correlation develops in the two-body denisty. The pair-potential folded with this anti-correlation is finite at zero relative distance, so improves this approach the high-density behavior of the equation of state. For confining forces between the constituents of quark-gluon plasma or an effectively massive quark matter the bare pair-potential is divergent at large distances. At low color density this confining force induces a (positive) correlation towards neutral clusters. A nearest neighbour approximation to the effective potential thus improves the low density behavior of the equation of state.

A very simple example of this is the inclusion of string like interaction, with an energy density contribution

$$\Delta e = n\sigma\langle \ell \rangle \propto n^{2/3}. \tag{2}$$

This result, however intuitive due to $\langle \ell \rangle \propto n^{-1/3}$, can be obtained more rigorous[1, 2, 3]. The approach is similar to strong coupling phenomena in solid state physics, where an effective potential is constructed from the naked interaction by weighting each interquark distance r (string length) with the probability of finding the nearest neighbour of corresponding colour:

$$v_{\text{eff}}(r,n) = v(r)g(r,n), \tag{3}$$

with

$$g(r,n) = \exp\left(-\frac{4\pi r^3 n}{3N_c}\right) \tag{4}$$

being the unnormalized nearest neighbour distribution function and N_c the number of colors. The energy density contribution is given by

$$\Delta e(r,n) = \frac{n^2}{N_c}\int v_{\text{eff}}(r,n)d^3r. \tag{5}$$

For the string energy, $v(r) = \sigma r$, we get

$$\Delta e(r,n) = \left(\frac{3N_c}{4\pi}\right)^{1/3}\Gamma(4/3)\sigma n^{2/3} \approx 0.63\sigma n^{2/3}. \tag{6}$$

Let us discuss the behavior of such equations of state, i.e. those with nontrivial density dependent corrections to the ideal gas. In the mean field approximation the Hamiltonian is given by

$$\mathcal{H} = u(n) + \sum_i (e_i + u_i(n))n_i \tag{7}$$

with density-dependent quasi-particle spectra and "mean" correction to the total Hamiltonian $u(n)$. Consistency requires, that

$$\begin{aligned}
\frac{\partial u}{\partial n_i} + \sum_j \frac{\partial u_j}{\partial n_i}n_j &= 0, \\
\frac{\partial u}{\partial T} + \sum_j \frac{\partial u_j}{\partial T}n_j &= 0.
\end{aligned} \tag{8}$$

These requirements are automatically fulfilled if we consider a density dependent modification of the free energy:

$$F(N,V,T) = \sum_i F^{\text{id}}(N_i,V,T) + Vb(N/V). \tag{9}$$

A look on the derived thermodynamical quantities (by a given temperature T, volume V and particle numbers $Vn = N = N_1, N_2, \ldots$),

$$\begin{aligned}
\mu_i = \frac{\partial F}{\partial N_i} &= \mu_i^{\mathrm{id}} + \frac{\partial b}{\partial n_i}, \\
S = -\frac{\partial F}{\partial T} &= S^{\mathrm{id}} - V\frac{\partial b}{\partial T}, \\
E = F + TS &= E^{\mathrm{id}} + V\left(b - T\frac{\partial b}{\partial T}\right), \\
p = -\frac{\partial F}{\partial V} &= p^{\mathrm{id}} - b + \sum_j n_j \frac{\partial b}{\partial n_j},
\end{aligned} \tag{10}$$

reveals that the requirements (8) can be fulfilled if

$$\begin{aligned}
0 &= \frac{\partial b}{\partial T}, \\
u_i &= \frac{\partial b}{\partial n_i}, \\
u &= b - \sum_j \frac{\partial b}{\partial n_j}.
\end{aligned} \tag{11}$$

A few examples of such EOS follows.

1. **MIT bag model** chooses $b = B$ constant, whence $u = B$, $u_i = 0$ featuring a bag pressure, but no mean field: $p = aT^4 - B$, $e = 3aT^4 + B$ is unstable below a critical temperature due to $p < 0$.

2. **Mean field models** consider $b = \sum_i n_i B_i$, containing no bag contribution $u = 0$ but a mean field correction $u_i = B_i$ for each particle species. The pressure is that of an ideal gas, the corresponding chemical potentials are shifted by B_i: this way some components can be favored or disfavored.

3. **String like EOS** with $b = \sigma n^{2/3}$ shows both effects: $u = \frac{1}{3}\sigma n^{2/3}$ and $u_i = \frac{2}{3}\sigma n^{2/3}$. This EOS leads to $p = nT - u \approx aT^4 - bT^2$ and $e \approx cT^4 + dT^2$ behavior describing a system which is unstable below a given temperature. The chemical potential $\mu = T\log(n/aT^3) + \frac{2}{3}\sigma n^{2/3}$ (in the Boltzmann approximation) has no zeros for low temperature signalling that no chemical equilibrium can be achieved. In this case all quarks become eliminated from the system. (Due to the entropy growth, $\dot{n} < 0$ for $\mu > 0$.)

1.3 Correlations and Equation of State

Using equations of state which include interaction, one may expect that the type of this interaction, i.e. whether it is repulsive or attractive, short range or long range, influences the behavior of correlations, as well. In fact there is a general method estimating the correlation lengths from the equation of state. The following presentation follows that of L. Diósi and B.Lukács [4, 5].

In the large volume limit $V \to \infty$ the equation of state is given by the entropy density as a function of all extensive densities

$$S = Vs(x^1, x^2, \dots x^n), \tag{12}$$

which is maximal in the equilibrium state $x = x_0$. The correlation of density fluctuations near to this state is defined by the inverse of the second derivative matrix in a parabolic (Gaussian) approximation,

$$\mathcal{P} \propto e^S \propto e^{-\frac{1}{2}(x-x_0)^i V g_{ik} (x-x_0)^k}, \tag{13}$$

from a Taylor expansion giving

$$g_{ik} = -\frac{\partial^2 s}{\partial x^i \partial x^k}. \tag{14}$$

Denoting the inverse of this "metsric tensor" by g^{ik} we arrive at the simple result already published by Albert Einstein [6]:

$$\langle (x-x_0)^i (x-x_0)^k \rangle \propto \frac{1}{V} g^{ik}(x_0). \tag{15}$$

This is true for any system in the large volume limit; deviations from this rule can be traced back to physical correlations. In order to get an estimate of this one assumes that the above Gaussian probability distribution is a solution of an abstract Fokker-Planck equation,

$$\frac{\partial}{\partial \tau} P(\tau, x|x_0) = \frac{\partial^2}{\partial x^i \partial x^k} \left(g^{ik}(x) P(\tau, x|x_0) \right). \tag{16}$$

Here $\tau = 1/V$ is the inverse volume, the expansion parameter in the thermodynamical limit. The "initial" condition at $\tau = 0$ is the general result (15),

$$P(0, x|x_0) = \delta^{(n)}(x - x_0). \tag{17}$$

The quadratic correlation of fluctuations can then be obtained by using the solution of the eqs.(16). An expansion up to $\mathcal{O}(1/V^2)$ terms gives

$$\langle (x-x_0)^i (x-x_0)^k \rangle \propto 2 \left(\tau g^{ik}(x_0) + \frac{\tau^2}{2} \Box g^{ik}(x_0) \dots \right). \tag{18}$$

Here

$$\Box g^{ik} = g^{rs}(x_0) \frac{\partial^2}{\partial x^r \partial x^s} g^{ik}(x_0). \tag{19}$$

Relative deviations from the universal correlation law can now be obtained from the eigenvalues of the matrix

$$Q^i_j = (\Box g^{ir}) g_{rj}, \tag{20}$$

Let us review some examples.

- ideal gas,

$$s = n\left(\frac{3}{2}\ln e - \frac{5}{2}\ln n + K\right) \tag{21}$$

leads to

$$\begin{aligned} \langle \delta e^2 \rangle &= \frac{2}{V}\frac{5}{3}\frac{e^2}{n}\left(1 + \frac{2}{3nV} + \dots\right), \\ \langle \delta n^2 \rangle &= \frac{2}{V} n\left(1 + \dots\right). \end{aligned} \tag{22}$$

This points out a thermal correlation volume of $v = 4/(3n)$. This is not due to interaction, since we are dealing with an ideal gas, but due to statistics: keeping the temperature constant the internal energy density fluctuates.

- black body radiation, from $e = aT^4$ follows

$$s = be^{3/4}. \tag{23}$$

Here one obtains $v = (5/2a)T^{-3}$, which is in the order of the thermal wavelength.

- critical point,

$$g_{ee} = -\frac{1}{T^2}c_V \propto (T - T_c)^a, \tag{24}$$

is the assumed scaling of the specific heat near to the critical temperature. Following the above method one obtains

$$v \approx \xi^d \approx \frac{\Box g^{ee}}{2g^{ee}} \approx (T - T_c)^{a-2}, \tag{25}$$

with d being the spatial dimension. Comparing this with the critical behavior of the correlation length

$$\xi \approx (T - T_c)^{-\nu} \tag{26}$$

one arrives at the well known mean field result

$$\nu d = 2 - a. \tag{27}$$

- In the van der Waals gas there is an already non-trivial correlation in density fluctuations stemming from the modification of the entropy by $n\ln(1 - n/n_0)$,

$$\begin{aligned} v^{(e)} &= \frac{\text{const.}}{n}\left(1 + \mathcal{O}(n/n_0)\right), \\ v^{(n)} &= -\frac{\text{const}}{n_0} + \mathcal{O}(n/n_0^2). \end{aligned} \tag{28}$$

Here an anticorrelation proportional to the excluded volume $1/n_0$ is obtained.

- Finally in the string like equation of state, e is replaced by $e - \sigma n^{2/3}$ in the ideal gas formula. In the high-density expansion we obtain

$$\begin{aligned} v^{(e)} &= \frac{\text{const}}{n}\left(1+\mathcal{O}(\sigma n^{2/3}/nT)\right), \\ v^{(n)} &= \text{const}\frac{\sigma}{T}n^{-1/3}+\ldots. \end{aligned} \tag{29}$$

In our last example, the number density correlation is positive in the high density approximation, featuring a long range attractive force, which is screened. There is, however, in the case of attractive long range forces, like strings, a mechanical instability when the pressure becomes negative. Furthermore there is no chemical equilibrium below a given temperature as discussed at the beginning of this lecture. Finally the correlation of density fluctuations (the inverse "metric" tensor) diverges at

$$\frac{\sigma}{Tn^{1/3}} = \frac{16}{9}. \tag{30}$$

Here we reach the frontier of the thermodynamical instability having passed earlier the chemical and mechanical instability lines.

Summarizing this lecture the confinement can be phenomenologically taken into account by string-like interactions, which leads to peculiar equation of state for the constituent quark matter. The reach of instabilities below a given density and temperature forces the building of color neutral clusters. This model can be used in far from equilibrium calculations as well as for near-equilibrium transport phenomena. The utilization of such an equation of state for the description of the hadronization of a quark matter will be the topic of the next lecture.

2 The Transchemistry Model

In the research of ultra-relativistic heavy ion collisions the prime attempts to describe the hadronization assumed, that the precursor quark matter consists of non-interacting massless quarks and gluons [7, 8, 9]. In place of these early image of free quarks and gluons (plasma) - which was based on thermodynamical studies of the pure nonabelian gauge theory on the lattice - gradually the picture of a quark matter emerges, containing effective propagators and interaction vertices [10, 11, 12]. At the characteristic energy scale of CERN SPS heavy ion experiments ($\sqrt{s}/2 \approx 10$ GeV/nucleon) the dressed gluons are heavier than the quarks ($M_g \approx 600 - 800$ MeV, $M_q \approx 150 - 300$ MeV) [12], and both values are bigger than the temperature ($T \approx 160$ MeV). Therefore the number of quarks overweight that of the gluons and can be treated non-relativistically. On the ground of these theoretical indications we expect that in the CERN heavy ion experiments not an ideal quark gluon plasma, but a constituent quark plasma (**CQP**), which contains antiquarks too, is formed in some intermediate state of the reaction (see the ALCOR model, Ref. [13, 14]).

For the description of heavy ion reaction products at SPS a purely hadronic interpretation of bulk experimental results was also suggested [15]. This alternative interpretation, however, has problems in explaining the process of the creation of new hadrons, especially the short time scale. Namely, the hadronic processes have characteristic times of several tens of fm/c [9, 16], while the typical heavy ion reaction time at SPS energy is about $1-2$ fm/c [17]. Processes on the quark level on the other hand have equilibration times of the order of $0.1-2$ fm/c [7, 8, 18].

The **CQP** picture has some advantages in comparison with the quark-gluon plasma scenario too: In the hadronization of a quark-gluon plasma the principles of color confinement and entropy generation can be both satisfied only with the assumption of an extreme growth of the reaction volume [19]. Further, a slow first order transition through near-equilibrium states would need too long time (up to 50 fm/c), due to the re-heating [20].

In this paper we assume that a massive quark matter, the **CQP**, is formed in heavy ion reactions at SPS energy, which is in thermal but not necessarily in chemical equilibrium. The evolution of this **CQP** is followed through a set of coupled time dependent differential equations for the temperature and chemical composition. The construction of the equations requires relations between the different equilibrium particle numbers at an actual temperature as input. These input values are determined by the equation of state.

First we review the derivation of a set of rate equation for a mixture of ideal gases. The familiar energy-momentum conservation

$$\partial_\nu T^{\mu\nu} = 0, \tag{31}$$

with

$$T^{\mu\nu} = (\varepsilon + p) u^\mu u^\nu - p g^{\mu\nu}, \tag{32}$$

being the energy-momentum tensor of a perfect fluid with flow four-velocity u_μ, local energy density ε and pressure p, has two interesting projections: one is parallel to the four-velocity,

$$u_\mu \partial_\nu T^{\mu\nu} = \partial_\nu(\varepsilon u^\nu) + p(\partial_\nu u^\nu) = 0, \tag{33}$$

and the other is orthogonal to this,

$$(u^\mu (u^\nu \partial_\nu) - \partial^\mu)\, p + (\varepsilon + p)(u^\nu \partial_\nu) u^\mu = 0. \tag{34}$$

The former - expressing local energy conservation - can be casted into the suggestive form

$$dE + pdV = 0 \tag{35}$$

using an infinitesimal volume element, $dV = (\partial_\mu u^\mu) V d\tau$, the total internal energy, $E = \varepsilon V$, and the parametric derivation with respect to the time-variable in the co-moving fluid cell,

$$\frac{d}{d\tau} = u^\nu \partial_\nu \ . \tag{36}$$

Starting from the first principal theorem of thermodynamics

$$dE = TdS - pdV + \sum_i \mu_i dN_i, \tag{37}$$

and using eq.(35) we arrive at the following change of rate of the total entropy:

$$\dot{S} = -\sum_i \frac{\mu_i}{T} \dot{N}_i, \tag{38}$$

where the 'dot' stands for the time derivative ($\dot{S} = dS/d\tau$). The chemical potentials μ_i can generally be derived from the equation of state.

We consider a flow pattern given by the Bjorken-flow

$$u_\mu = \left(\frac{t}{\tau}, \frac{z}{\tau}, 0, 0 \right) . \tag{39}$$

Here

$$\tau^2 \quad = \quad t^2 - z^2, \tag{40}$$

and the four-velocity is normalized to $u_\mu u^\mu = 1$ and its four-divergence is

$$\partial_\mu u^\mu = \frac{1}{\tau} . \tag{41}$$

The energy density ϵ and the pressure p depend only on τ and the flow is stationary. Corrections stemming from a mild radial flow also can be worked out, but we do not use these corrections here. The effective dimensionality of the flow is 1 in this case.

Since we deal with a system of rate equations for particle species numbers N_i occupying a common reaction volume V at temperature T, the generating thermodynamical functional is the free energy, $F(V, T, N_i)$. The chemical potentials are given by

$$\mu_i = \frac{\partial F}{\partial N_i}, \tag{42}$$

the pressure by

$$p = -\frac{\partial F}{\partial V}, \tag{43}$$

the entropy by

$$S = -\frac{\partial F}{\partial T}, \tag{44}$$

and finally the internal energy is

$$E = F + TS. \tag{45}$$

As a starting point we consider a mixture of ideal gases of massive quarks, diquarks, mesons and baryons, and their respective anti-particles. The corresponding free energy is

$$F_{\rm id} = \sum_i TN_i \left(\ln \frac{N_i}{N_{i,\rm th}} - 1 \right) \; + \; \sum_i m_i N_i, \tag{46}$$

with Maxwell-Boltzmann statistics for the non-relativistic massive matter:

$$N_i^{\rm th} = V d_i \int \frac{d^3p}{(2\pi)^3} \, e^{-p^2/2m_iT}. \tag{47}$$

Here $d_i = (2s_i + 1)c_i$ are spin and color degeneracy factors. The chemical potentials in an ideal gas mixture are

$$\mu_{i,\mathrm{id}} = T \ln \frac{N_i}{N_i^{\mathrm{th}}} + m_i. \tag{48}$$

The total entropy is given by

$$S_{\mathrm{id}} = \sum_i N_i \left(\frac{5}{2} - \ln \frac{N_i}{N_i^{\mathrm{th}}} \right). \tag{49}$$

The energy and pressure of such an ideal, non-relativistic mixture is given by

$$\begin{aligned} E_{\mathrm{id}} &= \sum_i \left(m_i + \frac{3}{2} T \right) N_i, \\ p_{\mathrm{id}} &= \sum_i N_i \frac{T}{V}. \end{aligned} \tag{50}$$

2.1 String-like interaction in the Equation of State

In order to take into account confinement effects we now apply the following confinement principle: all particles carrying color charge (quarks, diquarks, anti-quarks and anti-diquarks) will be penalized by a free energy contribution stemming from strings. These strings on the other hand are screened in the dense quark matter, having an average (and maximal) length determined by the density. The number of strings is proportional to a weighted sum of the number of color charges,

$$Q = \sum_i q_i N_i, \tag{51}$$

Here it is $q_i = 0$ for hadrons, $q_i = 1/2$ for quarks and anti-quarks, and $q_i = 3/4$ for diquarks and anti-diquarks. The higher effective charge of diquarks reflects a possibly higher number of in-medium partners, to which a string is stretched.

The average length L of a string depends on the density of colored objects, as $L = n_c^{-1/3}$, where

$$n_c = \sum_{i \in c} N_i / V, \tag{52}$$

where the summation $i \in c$ excludes color neutral particles (hadrons). So the free energy of the ideal quark matter - hadron matter mixture, $F = F_{\mathrm{id}} + \Delta F$, is supplemented by the following contribution of strings:

$$\Delta F = \sigma_s n_c^{-1/3} Q, \tag{53}$$

with the effective string tension $\sigma_s \approx 1.0\ GeV/fm$. This is a generalization of the string equation of state already discussed in the first lecture.

This additional free energy comprises the non-ideality of the equation of state we use. Since this addition is proportional to the volume V and the rest depends on densities only, it satisfies thermodynamical consistency requirements [21] due to its construction.

While there is no new contribution to the entropy,

$$S = S_{\rm id}, \tag{54}$$

the pressure, the energy and the chemical potentials of colored ($q_i \neq 0$) particles receive important modifications:

$$\begin{aligned} p &= p_{\rm id} - \frac{1}{3}\sigma_s n_c^{-1/3}\frac{Q}{V}, \\ E &= E_{\rm id} + \sigma_s n_c^{-1/3} Q, \\ \mu_i &= \mu_{i,{\rm id}} + \sigma_s n_c^{-1/3}(q_i - \frac{1}{3}\overline{q}), \end{aligned} \tag{55}$$

with $\overline{q} = Q/(Vn_c)$. Hadronic chemical potentials have no modifications at all.

This non-ideal completion of the equation of state influences both the expansion and cooling and the changes of particle composition. Since the entropy is not changed by the introduction of the interaction term (see. eq. (54)) therefore

$$TdS = TdS_{\rm id} \ . \tag{56}$$

From this equation, using eq. (37) we obtain

$$dE + pdV - \sum_i \mu_i dN_i = (dE + pdV)_{\rm id} - \sum_i \mu_{i,id} dN_i \ . \tag{57}$$

Applying eq. (35), the non-ideal cooling law becomes

$$(dE + pdV)_{\rm id} + \sum_i (\mu_i - \mu_{i,{\rm id}})\, dN_i = 0 \ . \tag{58}$$

Accordingly we get a new generic term due to the non-ideal equation of state,

$$\begin{aligned} \frac{\dot{T}}{T} &= -\frac{2}{3}\frac{\dot{V}}{V} - \frac{\sum_i \dot{N}_i}{\sum_i N_i} - \frac{2}{3}\frac{\sum_i (m_i/T)\dot{N}_i}{\sum_i N_i} \\ &- \frac{2}{3}\frac{\sum_i (\mu_i/T - \mu_{i,{\rm id}}/T)\dot{N}_i}{\sum_i N_i} \end{aligned} \tag{59}$$

The additional term has the form

$$\sum_i \frac{\mu_i - \mu_{i,id}}{T}\dot{N}_i = \frac{\sigma_s n_c^{-1/3}}{T}\sum_{i\in c}(q_i - \frac{1}{3}\overline{q})\dot{N}_i \ . \tag{60}$$

This term is negative if color charges are eliminated from the mixture. Therefore color confinement, causing an extra suppression of equilibrium numbers of quarks and alike particles, re-heats the expanding fireball as well as the "normal" chemistry of the ideal quark - hadron mixture. The more one suppresses color charges with respect to an ideal mixture the more re-heating occurs during hadronization. This, of course, works against the hadronization process. The only physical effect besides a fast expansion - which has, however, kinematical limits stemming from scaling relativistic expansion - that can cool the mixture sufficiently is rest-mass production. The color charge eliminating hadronization therefore must be accompanied by the production of heavy hadron resonances. (Rest mass production due to quark pair or gluon creation would not reduce color.) Since in our equation of state we have an explicit interaction energy between the quarks, our effective quark masses should be less than that given in Ref.[12]. We shall use the following values: ($m_u = [m_{u0}^2 + m_{th}^2]^{1/2}$, $m_d = [m_{d0}^2 + m_{th}^2]^{1/2}$, $m_s = [m_{s0}^2 + m_{th}^2]^{1/2}$, with thermal mass $m_{th} = 0.15$ GeV and $m_{u0} = m_{d0} \approx 0, m_{s0} = 0.15$ GeV. The clusters have a mass according to the average mass extra to the summed valence quark masses of the two lowest lying hadron multiplets: the pseudoscalar and vector meson nonets and the baryon octet and decuplet, respectively.

2.2 DYNAMICS OF HADRONIZATION

2.2.1 Initial state

The initial energy density — distributed along the beam direction between $-\tau_0 \sinh \eta_0$ and $\tau_0 \sinh \eta_0$ — can be related to the center of mass bombarding energy $\sqrt{s}$ in the experiment,

$$\varepsilon_0 = \frac{\sqrt{s}}{\pi R_0^2 \tau_0 2\mathrm{sh}\eta_0}. \tag{61}$$

On the other hand the initial invariant volume dual to $d\tau$ at constant $\tau = \tau_0$ is given by

$$V_0 = \pi R_0^2 \tau_0 2\eta_0. \tag{62}$$

The initial internal energy (i.e. the energy without the collective flow of a fluid cell) at $\tau = \tau_0$ is therefore less than $\sqrt{s}$ for finite η_0:

$$E_0 = \varepsilon_0 V_0 = \frac{\eta_0}{\mathrm{sh}\eta_0}\sqrt{s}. \tag{63}$$

At the CERN SPS experiment $\eta_0 \approx 1.75$ (due to some stopping), $R_0 \approx 7$ fm, $\tau_0 \approx 0.8$ fm and we obtain $V_0 \approx 431$ fm^3 and $E_0 \approx 2.13$ TeV. Compared to the total energy of about $\sqrt{s} = 3.4$ TeV (carried by about 390 participating nucleons in a central Pb-Pb collision) approximately two third of the energy is invested into rest mass of newly produced particles and thermal motion and and one third into the flow.

Comparing this with an alternative expression for the thermal energy of an ideal massive quark matter,

$$E_0 = \sum_i N_i(0)(m_i + \frac{3}{2}T), \tag{64}$$

one can estimate the initial temperature at the beginning of hadronization. Using our standard values for the incoming quark numbers [22] $N_u(0) = 544$, $N_d(0) = 626$, further, assuming that 400 $u\overline{u}$, 400 $d\overline{d}$ and, with $f_s = 0.21$, 168 $s\overline{s}$ quark anti-quark pairs are created in one central collision, we get from the above equation $T_0 = 0.18$ GeV. We use these numbers for the newly produced quark pairs in order to arrive at the experimentally measured hadron and strange particle numbers.

2.2.2 Hadronization processes

Chemical equilibrium is not supposed initially, rather a definite over-saturation of quarks in the reaction volume. The initially missing color-neutral hadron states - mesons and baryons - are formed due to quark fusion processes in a non-relativistic Coulomb potential. The rates for different flavor compositions differ mainly due to the different reduced masses of quark anti-quark or quark diquark pairs. First of all this influences the Bohr radius in the Coulomb potential [13]. Of course, the presence of a medium - which establishes the necessary momentum balance after the fusion - also influences the hadronization rate. The cross section for such a $2 \to 1$ process in medium is

$$\sigma = \left(\frac{\rho}{a}\right)^3 \frac{16M^2\sqrt{\pi}\alpha^2}{\left(\vec{p}^2 + 1/a^2\right)^2} \tag{65}$$

with $a = 1/(\alpha m)$ Bohr radius of the $1s$ state in the Coulomb potential and ρ is the Debye screening length [13]. Here $\vec{p}$ is the relative momentum of the hadronizing precursors, m is their reduced mass and M is the total mass.

The coupling constant we are using is a function of the relative momentum according to the formula

$$\frac{1}{\alpha(p)} = \frac{1}{\alpha_0} + \beta_{\rm QCD} \log \frac{p^2}{\Lambda^2_{\rm QCD}} \tag{66}$$

as long as $\alpha(p) < \alpha_0$. At smaller momenta it levels off at α_0. Here

$$\beta_{\rm QCD} = \frac{1}{4\pi}\left(\frac{11}{3} - 2N_F\right) \tag{67}$$

is the beta-parameter of the one loop beta-function occurring in the charge renormalization process in perturbative QCD. The function (66) is a good phenomenological approximation and has the correct infrared and ultraviolet asymptotics. The value $\alpha_0 \approx 1.4$ is taken in order to fit the gluon condensate strength in vacuum.

The medium effect is parameterized in all cross sections by $\rho \approx 0.2 - 0.3$ fm in a flavor independent way. If the hadronization process is fast enough, the prehadron numbers (i.e. hadron numbers before resonance decay) become proportional to the two-body reaction rates. Since quark fusion does not change the number of valence quarks during the hadronization the fast hadronization limit leads to the ALCOR model [13].

The relative momenta are taken from a random Gaussian distribution,

$$d\mathcal{P}(\vec{p}) \propto e^{-p^2/2mT} d^3p, \tag{68}$$

at temperature T and reduced mass m. This method allows us both to simulate thermally averaged hadronization rates,

$$R = \langle \sigma \frac{|\vec{p}|}{m} \rangle, \tag{69}$$

or to follow the event by event variation of the quark - hadron composition. For a fast estimate of thermally averaged rates about $3 - 5$ points in the relative phase space suffice for each reaction at each time instant.

Although the above corrections to the equation of state help to reduce the equilibrium ratio of free quarks to those confined in hadrons, total color confinement would only occur after a long time when the mixture is cool and dilute. This is obviously not the case in relativistic heavy ion collisions. Therefore we also apply a *dynamic confinement* mechanism in our model: the medium screening length ρ occurring in the hadronization cross section will be related to strings pulled by color charges trying to leave the reaction zone. This way the screening length ρ is increased as the color density decreases: we keep, however, the product $\rho^3 N_c/V$ constant,

$$\rho(t) = \rho(0) * (N_c(0)/N_c(t))^{1/3} . \tag{70}$$

Here N_c stands for the number of colored objects (each in triplet or anti-triplet representation),

$$N_c = N_Q + N_{\overline{Q}} + N_D + N_{\overline{D}}. \tag{71}$$

As we shall discuss in the next chapter both color confinement mechanisms are necessary in order to achieve a pure hadronic composition in a short time by trans-chemical processes, while satisfying the requirements of the entropy growth and energy conservation.

2.2.3 Reaction network

What remains to specify the model is the system of rate equations describing the transformation of quark matter into hadronic matter. We consider $N_F = 3$ light quark flavors u, d and s.

There are $N_F(N_F+1)/2 = 6$ possible diquark flavors and the same number of anti-diquark flavors. The number of quark anti-quark flavor combinations is $N_F^2 = 9$ while that of quark or anti-quark triplet combinations is $N_F(N_F+1)(N_F+2)/6 = 10$. In the hadronizing quark matter we deal with altogether $2*3+2*6+9+2*10 = 47$ sorts of particles.

Let us generally denote quarks by Q, diquarks by D, mesons by M and baryons by B. The possible fusion reactions are:

$$\begin{aligned} Q + Q &\longrightarrow D, \\ \overline{Q} + \overline{Q} &\longrightarrow \overline{D}, \\ Q + \overline{Q} &\longrightarrow M, \\ Q + D &\longrightarrow B, \\ \overline{Q} + \overline{D} &\longrightarrow \overline{B}. \end{aligned} \tag{72}$$

Accordingly the number of reaction channels, $2*10+9+2*6 = 41$ is $2N_F = 6$ less than the number of particle sorts. Therefore in chemical equilibrium, when the above reactions are balanced by the respective decays, the number of all particles are under-determined.

This is fortunately not a problem, because the hadronization reactions under consideration do not create or annihilate elementary quark flavors, they just produce new combinations. There are therefore exactly $2N_F = 6$ quark and anti-quark flavor numbers, which are conserved by these reactions. They are determined by the initial state.

Our model is completed by the system of rate equations. Considering a general reaction of type

$$i + j \longrightarrow k$$

we account for the changes

$$dN_i = dN_j = -Adt, \qquad dN_k = +Adt, \tag{73}$$

cumulatively in each reaction. Here

$$A = R_{ij\to k} N_i N_j \left(1 - e^{\frac{\mu_k}{T} - \frac{\mu_j}{T} - \frac{\mu_i}{T}}\right) \tag{74}$$

with a thermally averaged rate $R_{ij\to k}$ (cf. eq.(69)). The changes stemming from different reactions accumulate to a total change of each particle sort in a time-step dt.

Inspecting the expression (74) it is transparent that an extra increase of a chemical potential suppresses the production or enhances the decay of the corresponding particle. This behavior ensures that

$$\dot{S} = -\sum_i \frac{\mu_i}{T} \dot{N}_i > 0, \tag{75}$$

for any complicated network of reactions. The approach to chemical equilibrium always produces entropy.

2.2.4 Hadronic decays

The set of rate equations describes the time evolution of the number of all involved particles. In order to get the final hadron numbers we integrate these equations until the number of colored particles becomes negligible. This way we obtain a number of hadronic resonances (in the present version the vector meson nonet and baryon decuplet). Finally hadronic decays are taken into account with the dominant branching ratios obtained from Particle Data Table [23]. We assume that secondary hadron-hadron interactions have a negligible effect on the finally observed hadronic composition.

The time evolution of the entropy and temperature is obtained by simultaneous integration of eqs.(73) and (58). The structure of the rate equations containing both creation and decay terms ensures that the entropy never decreases during the transition [30]. On the other hand the energy conservation is established by the effective cooling law eq.(58). The numerical study of this complex system of equations is presented in the next section.

2.3 Strange Particle Ratios at CERN SPS energy

In this section we present the results of the numerical solution of the set of the $41 + 2$ coupled differential equations. In the Figures the calculated time evolution of the temperature, entropy, internal energy and the different particle and antiparticle numbers are presented for a 158 GeV / nucleon Pb + Pb central collision. For the numerical solution the initial condition and the values of the parameters has to be specified. For the parameters describing the initial state we used those given in subsection 2.2.1, while for the parameters determining the dynamics of the hadronization we used the following values: $\rho = 0.2fm$, $\alpha = 1.4$. Both the quarks and diquarks vanished only in the case, if we used the value $q_d = 1.5$ for the effective diquark color string tension. The time evolution of different quantities calculated with this initial condition and parameters are shown in the Figures.

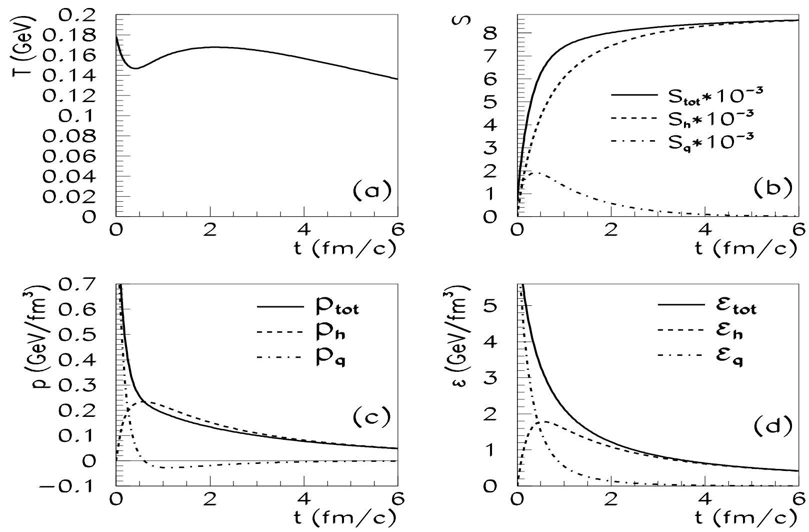

Fig. 1. The time evolution of the temperature T (a), the entropy S (b), the pressure p (c) and the energy density ε (d) of the system together with the partial contributions of quarks and hadrons.

From Fig. 1a we can see, that at the beginning of the hadronization there is a rapid decrease in the temperature due to the rest mass formation of the hadrons. Shortly after that, the reheating starts as an effect of color confinement (see eqs.(28) and (32)).The eq.(28) shows, that by removing two colored object to produce a colorless hadron, the associated string energy is also removed, and it has to appear in the thermal energy. Since this energy is inversely proportional to the one third root of the color density, this effect is stronger at smaller color density. Finally, as the hadronization is completed, the expansion bleeds to the cooling of the system. Fig. 1b shows, that the total entropy is monotonically increasing during the hadronization, while the contribution of colored particles (CQP) is gradually eliminated. In Fig. 1c one can observe an interesting pattern in the time evolution of the pressure. The partial pressure of the interacting CQP rapidly decreases as the number of quarks decrease. As the color density drops, this pressure becomes even negative. The increasing hadron partial pressure, however, overcompensates this negative value. At later times with the expansion of the ideal hadron gas the total pressure decreases. Due to this interplay, the total pressure falls steeply in the early period, it stays for a short while almost constant in the re-heating period, and finally drops slowly at the late expansion stage. Assuming an initial condition leading to slower hadronization, this balance is not so effective and in the time evolution of pressure a local minimum appears. The partial and total internal energy evolution, displayed in Fig. 1d, shows, that the hadronization is completed at 2 fm/c after the beginning of the process. The decrease of the internal energy is compensated by the work of pressure while making the flow (cf. eq.(35)), the total energy density drops due to the volume expansion like $\epsilon \propto 1/\tau$ at very late times only, when $p = 0$.

Fig. 2 shows the time evolution of different colored particles. The quark and antiquarks

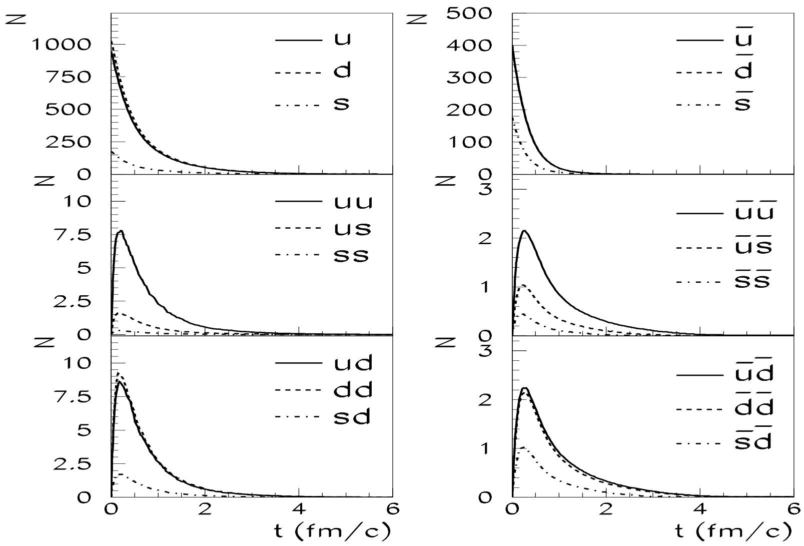

Fig. 2. The time evolution of the number of colored particles. The line styles of different flavor compositions are indicated in the respective figures.

numbers are monotonically decreasing functions of time. The diquarks are produced from the quarks, and then they contribute rapidly to the formation of baryons. That keeps their number always on a low level. In Fig. 3 the evolution of hadron numbers is shown. Here we did not take into account the decay of the resonances. Actually these time evolutions are the evolution of the constituent quark clusters, i.e. prime hadronic resonances, from which the experimentally observed particles emerge. It is clear from this Figures, that the mesons are formed faster than the baryons. This is understandable, if we consider, that the mesons are produced in a one step process, while the baryons are formed in a two step process: first the formation of diquarks and in a diquark quark reaction the formation of the baryon. In the ALCOR model the ratio of hadronic species are determined by the ratio of steepnesses of these curves. Since these curves do not cross each other, one can understand, why the algebraic ALCOR approach to the solution of rate equations is a good approximation. The difference, that at the very beginning the meson curves increase linearly with the time and the baryon curves start with a quadratic form, was taken into account in the ALCOR model by one single common factor, the so called baryon suppression factor.

In our model we calculate the number of all produced hadrons. In Table 1 the hadron numbers obtained with the Transchemistry model and those obtained with the ALCOR [22] and the RQMD [24] models are shown together with the few published experimental data. The present results of the ALCOR model are slightly different from the previously published ones [22], because here we considered the feeding of Λ^0 (and $\overline{\Lambda^0}$) particle multiplicities from Σ^0, Ξ^-, Ξ^0, Ω^- (and $\overline{\Sigma^0}$, $\overline{\Xi}^+$, $\overline{\Xi}^0$, $\overline{\Omega}^+$ respectively), as it was obtained in the experiments. The ALCOR fit

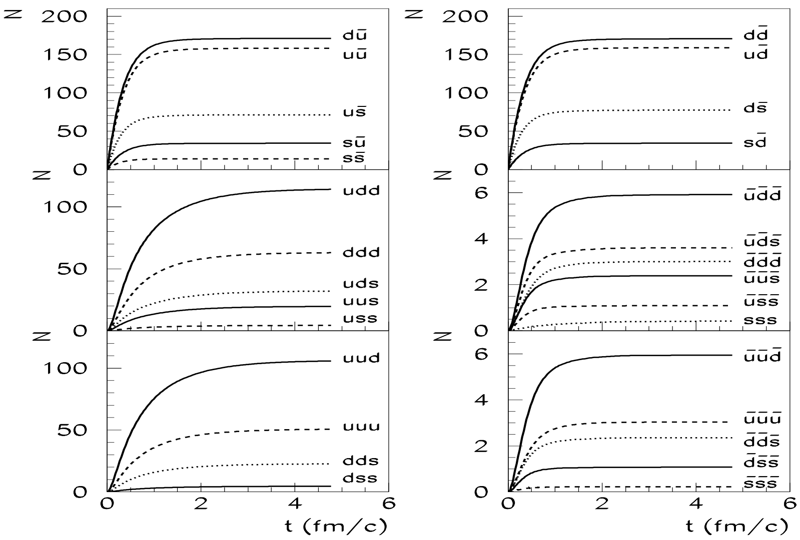

Fig. 3. The time evolution of the number of color neutral clusters consisting of quarks and/or anti-quarks indicated on the figures.

parameters to this new case are: $N_{q\overline{q}} = 391$, $N_{s\overline{s}} = 172$ and $\alpha_{\rm eff} = 0.97$ comparing to the earlier $N_{q\overline{q}} = 398$, $N_{s\overline{s}} = 175$ and $\alpha_{\rm eff} = 1.03$.

Table 2 shows a comparison for the multi-strange baryon ratios. While in many cases there are intriguing agreements, in some other cases there are some discrepancies. The reason for this may originate from two sources: i) the experimental data referred here are the production ratios in the overlap window of the detector acceptances. Thus, if the momentum distribution of the two particle sorts is not the same, then these ratios are not equal to the total number ratios. ii) these calculated values are more sensitive to the simplifying assumption, that the hadronization happens into the lowest lying baryon octet and decuplet and the two lowest lying meson nonet. We have committed this simplification, because the inclusion of other hadron multiplets would have multiplied the workload in the computer simulation. In our model we don't have such parameters with which the different particle ratios could be manipulated independently. The degree of the overall harmony between our results and the presently known experimental data seems to be promising and thus it could initiate the search for further signatures of the **CQP** state.

Here we presented a new model for the hadronization of a constituent quark plasma (**CQP**) based on rate equations in a quark matter - hadron matter mixture. The color confinement was taken into account by using consistently a plausible equation of state motivated by the string model. The role of the different physical processes entering into the hadronization was discussed. Our results presented in the Figures clearly show a very fast hadronization. This is mainly a consequence of the large hadronization rates, $R_{ij\to k}$ and of the fact that in the initial state the system is very far from equilibrium. Observing the shape of the time evolution of different hadron

Pb+Pb	NA49	TrCHEM.	ALCOR	RQMD
h^-	680^a	677.0	679.8	
π^+		581.7	590.6	692.9
π^0		617.0	605.9	724.9
π^-		613.1	622.0	728.8
K^+	76^*	79.58	78.06	79.0
K^0		79.58	78.06	79.0
$\overline{K}^0$		39.47	34.66	50.4
K^-	$\{32\}^b$	39.47	34.66	50.4
p^+		158.7	153.2	199.7
n^0		175.8	170.5	217.6
Σ^+		8.38	9.16	12.9
Σ^0		9.79	9.76	13.1
Σ^-		9.79	10.39	13.3
Λ^0		46.79	48.85	35.3
Ξ^0		4.40	4.89	4.2
Ξ^-		4.43	4.93	4.2
Ω^-		0.42	0.62	
$\overline{p}^-$		8.98	6.24	27.9
$\overline{n}^0$		8.93	6.24	27.9
$\overline{\Sigma}^-$		1.00	0.91	4.6
$\overline{\Sigma}^0$		1.09	0.91	4.6
$\overline{\Sigma}^+$		0.99	0.91	4.6
$\overline{\Lambda}^0$		5.24	4.59	10.7
$\overline{\Xi}^0$		1.08	1.12	2.0
$\overline{\Xi}^+$		1.08	1.12	2.0
$\overline{\Omega}^+$		0.22	0.35	
K_S^0	$\{54\}^{b,c}$	59.66	56.36	63.5
$p^+ - \overline{p}^-$	$\{145\}^a$	149.7	147.0	171.8
Λ^0-like	$\{50 \pm 10\}^b$	56.58	69.07	56.8
$\overline{\Lambda}^0$-like	$\{8 \pm 1.5\}^b$	6.34	8.12	19.3

Table 1. Total hadron multiplicities for $Pb + Pb$ collision at 158 GeV/nucleon bombarding energy. The displayed experimental results are from the NA49 Collaboration: estimated result ^{a} is from [25]; ^{b} is from [26]; ^{c} is from [27]; * is estimated from $\{K^-\}$ and $\{K_S^0\}$. Theoretical results are from the Transchemistry, ALCOR and RQMD [43] ("ropes + no rescattering" version) model. Here it is $\Lambda^0 -$ like $\equiv \Lambda^0 + \Sigma^0 + \Xi^- + \Xi^0 + \Omega^-$.

multiplicities, it became understandable, why the simpler algebraic approximation, applied in

Pb+Pb	WA97	TrCHEM	ALCOR
$\overline{\Lambda}^0/\Lambda^0$	0.128 ± 0.012	0.112	0.117
$\overline{\Xi}^+/\Xi^-$	0.266 ± 0.028	0.243	0.227
$\overline{\Omega}^+/\Omega^-$	0.46 ± 0.15	0.529	0.564
Ξ^-/Λ^0	0.093 ± 0.007	0.078	0.071
$\overline{\Xi}^+/\overline{\Lambda}^0$	0.195 ± 0.023	0.170	0.138
Ω^-/Ξ^-	0.195 ± 0.028	0.095	0.125

Table 2. Strange baryon and anti-baryon ratios measured by WA97 Collaboration [29] and obtained from Transchemistry and ALCOR model for $Pb + Pb$ collision at 158 GeV/nucl bombarding energy. The experimental data are the production ratios in mid rapidity at $p_T > 0\ GeV$.

the ALCOR model, works so well. The comparison with the existing experimental data indicate, that it is possible, that in the PbPb collision at SPS a piece of matter is formed, inside which the massive quarks and anti-quarks interact with a string like mean field.

Finally we emphasize, that this type of phenomenological investigations are necessary, as long as the hadronization of the quark matter as a non-equilibrium, non-static, non-perturbative process, cannot be described with the methods of the elementary field theory.

3 The Chromodielectric Model

In this lecture I report about a classical molecular dynamics approach on the quark level to hadronization. For the dynamical description, the classical limit of the chromodielectric model is used, where quarks and gluons are represented by extended but rigid charge distributions. The background fields are a scalar field and two abelian fields, corresponding to the two neutral colors in $SU(3)$. The six remaining, charged, gluons are treated as particles. We deal with these simplifications in order to be able to carry out a molecular dynamical calculation of about 400 quarks in an acceptable time. The essential confinement mechanism in this model is hidden in the scalar field self-interaction potential and the construction of the chromodielectric constant, whose particular dependence on the effective scalar field σ includes the main quantum-mechanical effect from QCD.

Since free quarks have never been observed experimentally, it is generally accepted that any physical state of finite energy has to be a singlet under color-$SU(3)$ transformations. This phenomenon is called color confinement. Since we know that classical ("tree-level") chromodynamics does not enforce color confinement, this has to be a quantum ("loop") effect, characteristic of a strongly interacting non-abelian gauge field theory. However, a proof of color confinement based solely on the QCD Lagrangian has not yet been given, mainly because it is too difficult to identify the relevant QCD degrees of freedom.

The chromodielectric (Friedberg-Lee) model [49] tries to mimic QCD's color confinement *on the classical level.* It introduces an additional scalar field σ that enforces color confinement in a conceivable way.

The Lagrangian reads

$$\mathcal{L} \;=\; \sum_f \bar{q}^f \left(i\not{D} - m_f \right) q^f - \frac{\kappa(\sigma)}{4} F^a_{\mu\nu} F^{\mu\nu a} + \frac{1}{2}(\partial_\mu \sigma)(\partial^\mu \sigma) - U(\sigma). \tag{76}$$

The symbol q^f denotes a quark spinor of flavor f; both the color and Dirac indices are suppressed, and the Feynman dagger notation $\not{D} = \gamma^\mu D_\mu$ is used. The covariant derivative $iD_\mu = i\partial_\mu - g_v A_\mu$ contains the color vector potential $A_\mu = A^a_\mu \frac{\lambda^a}{2}$, where the λ^a denote the eight Gell-Mann matrices. The color field tensor is defined as

$$F_{\mu\nu} \;=\; F^a_{\mu\nu} \frac{\lambda^a}{2} \;:=\; \frac{i}{g_v}[D_\mu, D_\nu]. \tag{77}$$

It obeys the classical chromodynamical field equation in a covariant medium with dielectric function $\kappa(\sigma)$,

$$[D_\mu, \kappa(\sigma) F^{\mu\nu}] \;=\; j^\nu, \tag{78}$$

with color current

$$j^\nu = g_v \sum_f \bar{q}^f \gamma^\nu \lambda^a q^f \frac{\lambda^a}{2}. \tag{79}$$

The quark field obeys a Dirac equation,

$$\left(i\not{D} - m_f \right) q^f \;=\; 0 \tag{80}$$

with a constituent quark mass m_f. The quarks can in principle be treated quantum-mechanically here, while the color and σ field are regarded as classical fields.

The scalar field σ obeys a Klein-Gordon equation with a fourth-order polynomial self-interaction $U(\sigma)$ and a complicated source term

$$\partial_\mu \partial^\mu \sigma + U'(\sigma) \;=\; -\frac{\kappa'(\sigma)}{4} F^a_{\mu\nu} F^{\mu\nu a} \tag{81}$$

Both functions U and κ are drawn schematically in Fig. 4.Note that there is no direct coupling between the quarks and the $\sigma-$field in this model.

The Lagrangian (76) describes a classical field theory with an explicit color confinement mechanism. The ingredients of this mechanism are the self-interaction term $U(\sigma)$, the dielectric function $\kappa(\sigma)$, and the color Gauss law. In this section, we utilize a simple example to explain how these three ingredients work together to enforce color confinement.

First note that in the vacuum of this theory, $\sigma \equiv \sigma_{vac}$ holds everywhere and thus $\kappa \equiv 0$. Now consider the static and color neutral quark-antiquark configuration depicted in Fig. 5.The charge distribution is given by $j_0(x) = j_0^3(x)\frac{\lambda^3}{2}$, i. e. it belongs to a $U(1)$ subgroup of $SU(3)$. The Gauss law reads for this case

$$\vec{\nabla} \cdot \vec{D}^3 \;=\; j_0^3. \tag{82}$$

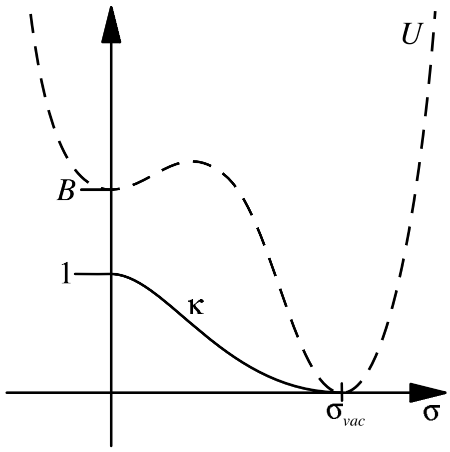

Fig. 4. Schematical graph of the functions $U(\sigma)$ and $\kappa(\sigma)$. Note that U is an energy density while κ is dimensionless. σ_{vac} denotes the value of the σ field in the physical vacuum (ground state).

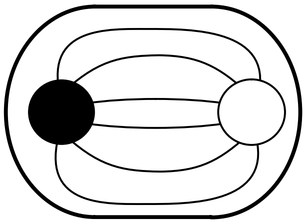

Fig. 5. A color flux tube.

It forces a color flux $\vec{D}^3 = \kappa(\sigma)\left(-\vec{\nabla}A_0^3 - \partial_t\vec{A}^3\right)$ to stretch from the quark to the antiquark. This flux cannot exist in regions where $\kappa = 0$, therefore the σ field has to deviate from its vacuum value, forming a tube (or bag) with $\sigma < \sigma_{vac}$ for the flux. Assuming U and κ are defined so that σ ends up being zero in the bag, the bag formation process costs an energy density B, which in turn can be interpreted as the vacuum pressure exerted on the bag.

Formulated differently, the vacuum pressure generated by $U(\sigma)$ and the coupling term κF^2 confines the color flux to a string — *U and κ together generate the color flux confinement*. On the other hand, the quarks cannot escape from this string because *the Gauss law demands a contiguous color flux to connect them.* Unless pair creation is allowed for, the resulting string can become arbitrarily long, causing the $q\bar{q}-$potential to rise linearly.

On our way to build a computer simulation of the chromodielectric model, we have to make several approximations. In doing so, we take care to preserve color confinement, since this is what we want to simulate.

We treat only the two commuting gluon fields $A_\mu^3\frac{\lambda^3}{2}$ and $A_\mu^8\frac{\lambda^8}{2}$ as classical fields; they correspond to two decoupled, color neutral fields which behave just like Maxwell fields. So from now on, the color index a is generally restricted to the values 3 and 8. This approach amounts to taking a $U(1) \times U(1)$ abelian subgroup of the full $SU(3)$ gauge group of QCD, and is therefore

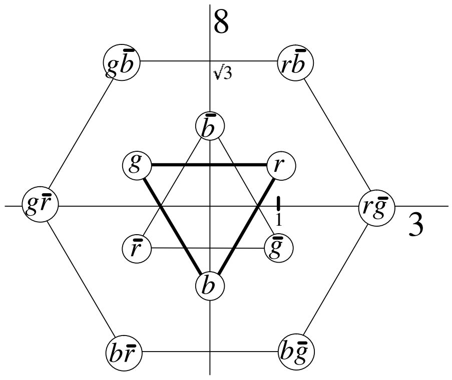

Fig. 6. Quark and gluon colors. The bold equilateral triangle corresponds to the quark colors, the other triangle to the antiquark colors, and the regular hexagon to the six charged gluons. The denotations r, g, b, $\bar{r}$, $\bar{g}$, $\bar{b}$ are chosen arbitrarily.

called the *abelian approximation*[58, 56]. However, in contrast to the cited works, we do not simply drop the other, charged, gluons. Instead, they are treated like the quarks and antiquarks: as classical charge distributions with a Gaussian shape of fixed width. Spin and isospin are accounted for by appropriate degeneracy factors. This changes the particle Lagrangian into the classical expression

$$\mathcal{L}_p^{class} \;=\; -\sum_i \rho_N(\vec{x}-\vec{x}_i) m_i \sqrt{1-\dot{\vec{x}}_i^{\,2}} \;-\; j^{\mu a} A_\mu^a \tag{83}$$

with the color current

$$j^{\mu a} \;=\; g_v \sum_i \rho_N(\vec{x}-\vec{x}_i) q_i^a \begin{pmatrix} 1 \\ \dot{\vec{x}}_i \end{pmatrix}. \tag{84}$$

The index i runs over all quarks, antiquarks and charged gluons in the system.

For the quarks, the color charges $q_i^{3,8}$ in (84) are equal to the diagonal entries in $\lambda^{3,8}$. Antiquarks carry the charge $-q_i^{3,8}$, and the gluons carry each the sum of one quark and one antiquark color charge. Fig. 6.summarizes the possible values.

The masses m_i are model parameters; our particular choices for them are listed and explained in Sec. 3. The function ρ_N is a Gaussian number density distribution of unit norm and RMS radius $\langle \vec{x}^2 \rangle = 3r_0^2$,

$$\rho_N(\vec{x}-\vec{x}_i) \;=\; \left(\frac{1}{2\pi r_0^2}\right)^{3/2} e^{-(\vec{x}-\vec{x}_i)^2/2r_0^2}. \tag{85}$$

In the present version of our model, particle production or annihilation is not yet included. In principle, it is no essential problem to implement them, once an appropriate probability density is at hand. This remains for future work.

If a quark-gluon plasma is formed in an ultrarelativistic heavy-ion collision, the droplet as a whole has to be a color-$SU(3)$ singlet. Since our numerical model respects only an abelian

$U(1) \times U(1)$ subgroup of the $SU(3)$ symmetry group, an "$SU(3)$ color singlet" is represented simply by a "white" cluster, i. e. one that is color neutral with respect to both the λ^3- and the λ^8-charge (cf. Fig. 6.).An $SU(3)$ color singlet is then built "automatically" by the presence of classical A^3_μ and A^8_μ fields, as solutions of (78). Our simulation therefore starts off from a large but white quark-gluon plasma droplet.

In nature, the hadronization process then divides the initial large cluster into a number of hadrons that are themselves separate color singlets. Correspondingly, our simulation is supposed to end up in a final state of small, white clusters that can be interpreted as hadrons. In this section, we investigate and classify the sorts of small clusters that we expect to find in the final state.

Imagine a small, white cluster of color charges. Suppose it cannot be subdivided into smaller but still white subclusters. Then, flux tubes bind the cluster together, forcing it to rotate or oscillate in a "yoyo" mode [56, 57]. Thus it will emit σ waves, which cool the cluster down. Finally, all the color charges are resting with respect to each other, being centered at the same point in space. If we choose the same color charge distribution width for all particle species, the final cluster's charge density will vanish identically; therefore, all fields will take on their repective vacuum values in this cluster.

Because of the vanishing of all fields, two such clusters that happen to be close to each other can neither attract nor repel, and a small relative momentum suffices to separate them spatially. Consequently, we may conclude that *the final state of our simulation must be a collection of irreducible white clusters*, i. e. white clusters that cannot be divided into white subclusters. It turns out that only a finite number of possible color combinations can form irreducible clusters, which enables us to classify them, according to Fig. 7.,as mesonic, baryonic and pure glue ball states. The latter occur as mesonic resonance states in the experimental observation.

When studying hadronization processes, our program checks at each timestep whether there are irreducible white clusters in the system. A "cluster" in the computational sense is a set of color charges located in a common σ field bag (defined here as a connected spatial domain with $\kappa > \frac{1}{2}$). The bag vanishes for cold clusters in our model (see Sec. 3), so if a set of charges is outside any σ field bag but very close in phase space, we treat it as a cluster as well. If the cluster is irreducibly white, i. e. possesses one of the color structures displayed in Fig. 7., it is considered to be a new hadron. The program then classifies the hadron according to its color structure, computes particle and field contributions to momentum and energy, removes the charges and field imprints from the simulation as well as possible, and generates a hadron, i. e. a white, non-interacting object that just proceeds on a straight path and may even leave the lattice.

To simplify the problem, we neglect the chromomagnetic $\vec{B}^{3,8}-$fields in our simulation (and thereby neglect the corresponding color waves). Although breaking Lorentz invariance, it is not as bad an approximation as it may seem: it is exact for static charge configurations like in the computation of the string tension (Fig. 8.);it is also exact for yoyo-like excitation modes of flux tubes in their rest frame[63]. Furthermore, the color confinement mechanism explained in Sec. 3 is not broken by this approximation. Finally, the color field waves cannot mediate forces or transfer energy between hadronic bags because the Poynting vector $\kappa\vec{E} \times \vec{B}$ vanishes anyway in the physical vacuum. So the neglection of $\vec{B}$ amounts to a neglection of some inner degrees of freedom of clusters that are nonessential for the confinement transition.

Neglecting $\vec{B}^a$, $\vec{E}^a$ can be derived from a single potential,

$$\vec{E}^a = -\vec{\nabla}\phi^a. \tag{86}$$

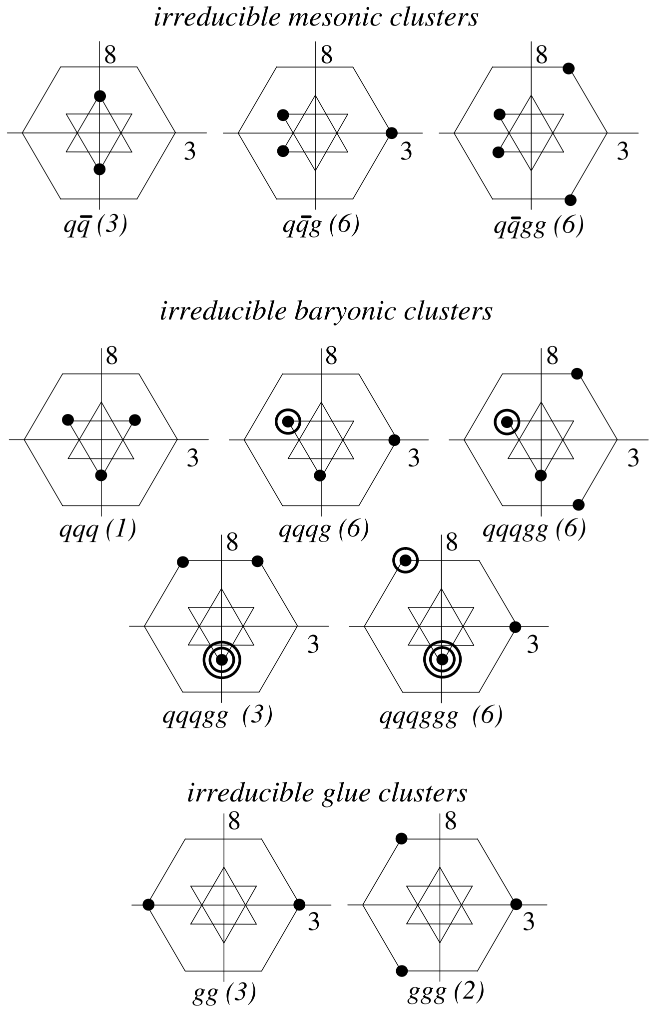

Fig. 7. Classification of irreducible white clusters in the color diagram of figure 3. Points and circles indicate the occupation number of each color state. Numbers in brackets indicate the color degeneracy of the diagram for each quark flavor combination.

The Gauss law, written in terms of ϕ^a, reads

$$\nabla \cdot (\kappa(\sigma)\nabla\phi^a) \;=\; -\rho^a. \tag{87}$$

This is still a constraint equation, modelling the constraint of quark confinement. It constitutes a boundary value problem that has to be solved at each timestep of the simulation. This has to be done carefully since the color electric flux is an essential ingredient of the confinement mechanism.

Note that (87) is singular in regions where κ vanishes; this is a major obstacle to numerical treatment. We overcome it in practice by choosing a nonzero but small value for κ_{vac} (see Sec. 3). Still, (87) is nearly singular and correspondingly difficult to solve. A well-tuned successive overrelaxation scheme (SOR) on a fixed grid with N^3 points, possessing at the very best a time complexity of $\mathcal{O}(N^4)$ [64], does not suffice here. Fourier transformation methods are excluded because of the nonconstant coefficient function $\kappa(\sigma)$. So we choose a fast solution algorithm based on the hierarchical basis multigrid method[65]. We are using a tetrahedral mesh of finite elements and take piecewise quadratic basis functions for the Ritz-Galerkin variational ansatz. During the multigrid iterations, the mesh is adaptively refined by bisection[66], which leads to block-diagonal matrices on each level of the multigrid scheme[67]. Refinement is performed only in those regions where the solution function varies with short wavelengths, e. g. close to the charges. This guarantees a certain precision of the solution ϕ^a independently of the structure of the sources ρ^a or the coefficient function $\kappa(\sigma)$.

Before studying dynamical properties, like the time evolution of a quark-gluon plasma, in the present model, let us briefly discuss our choice of model parameters, which is based solely on certain desired time-independent observables, namely the hadronic mass spectrum, and color flux tube properties.

We choose the same charge distribution radius $\sqrt{\langle \vec{x}^2 \rangle} = 0.7$ fm for all the various particle flavors. The model possesses in this case a particularly simple "hadron spectrum". Cold (unexcited) hadrons are white (color neutral) combinations of several particles centered at the same location. Their color charge distribution vanishes everywhere, therefore the fields all take on their vacuum values. Thus, the mass of such a hadron is simply the sum of the masses of its constituents. In order to obtain roughly the proper hadronic mass scales, we have chosen a nonstrange quark mass of 400 MeV, yielding a mass of 800 MeV for the $\rho-$meson and 1200 MeV for the nucleon. The other masses are all given in table 3. This table exhibits a reasonable agreement between model and experimental numbers; fine-tuning could certainly improve this even further.

Such a constituent quark model without any interaction contribution to hadronic ground state energies can never successfully describe the low masses of the light, strongly bound hadrons, like π or K mesons, or nucleons. It is interesting in this context that the experimental masses of the first excitations can be tuned in very well with roughly chosen quark masses (see table 3). Of course, this fit is not meant as a serious model of hadrons.

The parameters of the quartic potential $U(\sigma)$ and the dielectric function $\kappa(\sigma)$ are harder to fix since there is no well-known physical particle associated with σ. However, if we interpret $\sigma-$waves as pure glueballs with a mass of about $1400MeV$, we obtain $U''(\sigma_{vac}) = (1400MeV)^2$. Furthermore, the bag constant $B = (150MeV)^4$, and $\sigma_{vac} = 0.31\text{fm}^{-1}$ are chosen in order to get a low bag surface tension — which is easier to handle numerically — while still having a region with $U''(\sigma) < 0$, which is a necessary condition for a first order color deconfinement phase transition to occur. Our particular choices are motivated by studies of solitonic states in the model [54, 55]. Finally, we use

$$U(\sigma) \;=\; B + a\sigma^2 + b\sigma^3 + c\sigma^4 \tag{88}$$

with $a = 6.184\text{fm}^{-2}$, $b = -80.72\text{fm}^{-1}$, $c = 163.1$, $B = (150\text{MeV})^4$. For κ, it turns out that the simulation results are not very sensitive to its precise shape. As described in the last section,

particle	model mass	exp. mass	error
q	400	-	-
s	550	-	-
g	700	-	-
$\frac{1}{2}(N+\Delta)\ (qqq)$	1200	1086	+10.5%
$Y\ (qqs)$	1350	1385	-2.5%
$\Xi\ (qss)$	1500	1530	-2.0%
$\Omega\ (sss)$	1650	1672	-1.3%
$\rho\ (q\bar{q})$	800	770	+3.9%
$\omega\ (q\bar{q})$	800	782	+2.3%
$K^*\ (q\bar{s})$	950	892	+6.5%
$\Phi\ (s\bar{s})$	1100	1020	+7.8%
gg	1400	1400 ? 1	-

Table 3. Quark and gluon effective masses, and corresponding hadron masses [Particle Data Table]. All masses are measured in MeV. The symbol q denotes an up or down quark, s a strange quark, and g a gluon.

its only purpose is to couple the vacuum pressure generated by $U(\sigma)$ to the color flux tube. For doing this, the κ function has to take on a value much smaller than one near $\sigma \approx \sigma_{vac}$. Secondly, κ has to rise quickly to one where $U(\sigma) \approx B$, supporting our interpretation of B as bag constant. We use

$$\kappa(\sigma) \;=\; \frac{1}{\exp\left(\alpha\left(\frac{\sigma}{\sigma_{vac}}-\beta\right)\right)+1} \tag{89}$$

with $\alpha = 5$ and $\beta = 0.4$.

Finally, the strong coupling constant $\alpha_S = g_v^2/4\pi$ is chosen such that the $q\bar{q}$ string tension equals about 1 GeV/fm, a value that can be deduced from quarkonium spectroscopy [68]. Anticipating the results of the next section, we show in Fig. 8.that a value of $\alpha_S = 2$ results in a satisfactory numerical string tension.

3.1 Molecular Dynamical Simulation of Hadronization

When carrying out a molecular dynamic simulation on the quark-gluon level, one has to make compromises. Even using modern computers and state-of-the-art numerical methods, we cannot simulate systems larger than a few hundred of particles in a volume of $(25\text{fm})^3$. The entire simulation run takes finally about a 200 fm, corresponding to weeks of CPU time on a Pentium Pro 200 MHz system.

Due to the above mentioned restrictions we decided to simulate only a central part of the heavy-ion collision region, including about 400 quarks and gluons in an initial volume of about 100 fm^3. In real $Pb + Pb$ collisons at CERN SPS, about $3000 - 4000$ particles are present in the quark matter phase. We use the following scenario in order to gain a qualitative insight about

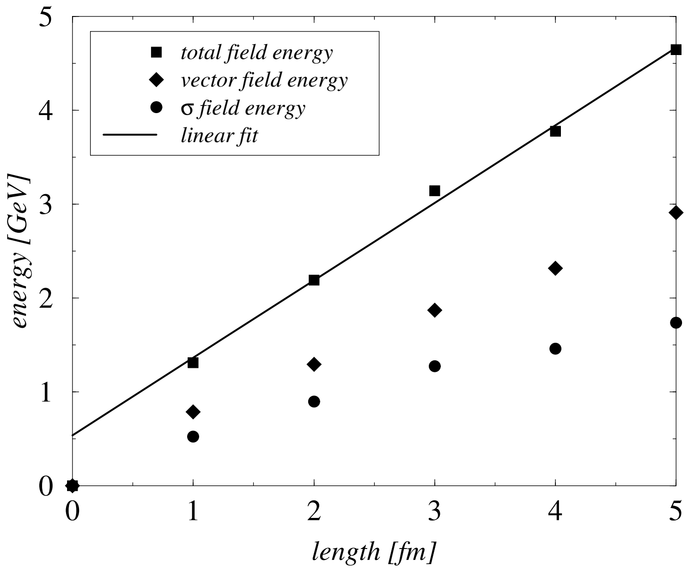

Fig. 8. The $q\bar{q}$-flux tube energy (σ and color field contributions) plotted against the separation distance of the quarks. The slope is about 1 GeV/fm.

the hadronization: a hot quark-gluon plasma initialized on top of a Bjorken-flow stretching from coordinate-rapidity $\eta_0 = -0.5$ to $\eta_0 = +0.5$.

The reaction volume is calculated assuming a radius of the initial sphere of $R_0 = 4$ fm or of the initial cylinder of $R_0 = 4$ fm, respectively. The initial energy density of $\varepsilon_0 = 2.5$ GeV/fm^3 is obtained from the total bombarding energy characteristic for SPS. The initial numbers of quarks and gluons are chosen according to non-relativistic Maxwell-Boltzmann statistics, using the respective masses and the initial temperature. The ratios of various flavor quarks and gluons are determined from equilibrium principles (law of mass action), with d_i the spin, color and flavor degeneracy. The resulting parton numbers are 133 light quarks, 40 strange quarks, the same numbers of respective antiquarks, and 44 gluons. The random Gaussian momenta (on top of the initialized flow pattern) satisfy

$$\left\langle \frac{p_{i,\mu}^2}{m_i} \right\rangle = T_0 \tag{90}$$

for each particle species and momentum components $\mu = x, y$ or z. We do not consider a nonzero quark chemical potential in the present work; furthermore there is no net color and no net strangeness in the system.

The basis of our identification of observables is the white cluster classification and hadronization mechanism described above. The total momentum and total energy of white clusters can be calculated from the individual four-momenta of its constituents and from the field energy carried by the classical vector fields. The mass of a cluster is defined by

$$M_{\rm clus}^2 = \left(E_{\rm field} + \sum_i E_i\right)^2 - \left(\vec{p}_{\rm field} + \sum_i \vec{p}_i\right)^2 . \tag{91}$$

Here,

$$\begin{aligned} E_{\rm field} &= \int d^3x \left(\frac{1}{2}\dot{\sigma}^2 + \frac{1}{2}(\vec{\nabla}\sigma)^2 + U(\sigma) + \frac{1}{2}\kappa(\sigma)\vec{E}^a\vec{E}^a\right) \\ \vec{p}_{\rm field} &= -\int d^3x\, \dot{\sigma}\vec{\nabla}\sigma. \end{aligned} \tag{92}$$

The mass distribution, dN/dM, tells the number of clusters with a mass between M and $M + dM$. The resolution dM of the mass binning is chosen to be $dM = 100$ MeV presently. If dM is too large, one cannot distinguish different particles; if it is too small, the statistics becomes too low. The above value is a compromise found by trial and error.

Further observables are the rapidity distribution dN/dy with

$$y = \frac{1}{2}\ln\frac{E + p_z}{E - p_z}, \tag{93}$$

and the transverse momentum distribution dN/dp_T with

$$p_T = \sqrt{p_x^2 + p_y^2}. \tag{94}$$

Collective flow and local temperature both affect these spectra: a strong longitudinal flow causes a plateau in the dN/dy distribution, while the slope of the transverse momentum spectra — if nearly exponential — includes both thermal and radially collective motion.

Finally, some global variables are of interest in order to obtain an approximate equation of state from the molecular dynamic simulation. A temperature-like quantity can be obtained by fitting the non-relativistic Maxwell-Boltzmann distribution to the momenta by inspecting

$$T_{i,\mu} = \langle p_{i,\mu}^2\rangle / m_i, \tag{95}$$

for a cluster of type i with mass m_i, and momentum direction $\mu = x, y$ or z. The approximate equality of these temperature-like parameters for different spatial directions μ reflects isotropy of the pressure, while its equality between different sorts of clusters i chemical and thermal equilbrium.

Fig. 9shows six snapshots of the time evolution for the Bjorken scenario. The simulation times of the snapshots are written inside the frames in units of fm; the frame diagonal is of length 45 fm. Quarks, gluons, and hadrons are drawn as spheres; for better visibility of the scene, the radius of a colored object is scaled down to one third of the actual RMS radius of the charge distribution (0.7 fm). Hadron radii reflect the bag volume formed by the σ field footprint of the hadronized cluster; they are scaled down to one half of their actual size. For white clusters without any σ field bag (see section 3), we draw a sphere of radius 0.35 fm. The σ field as well

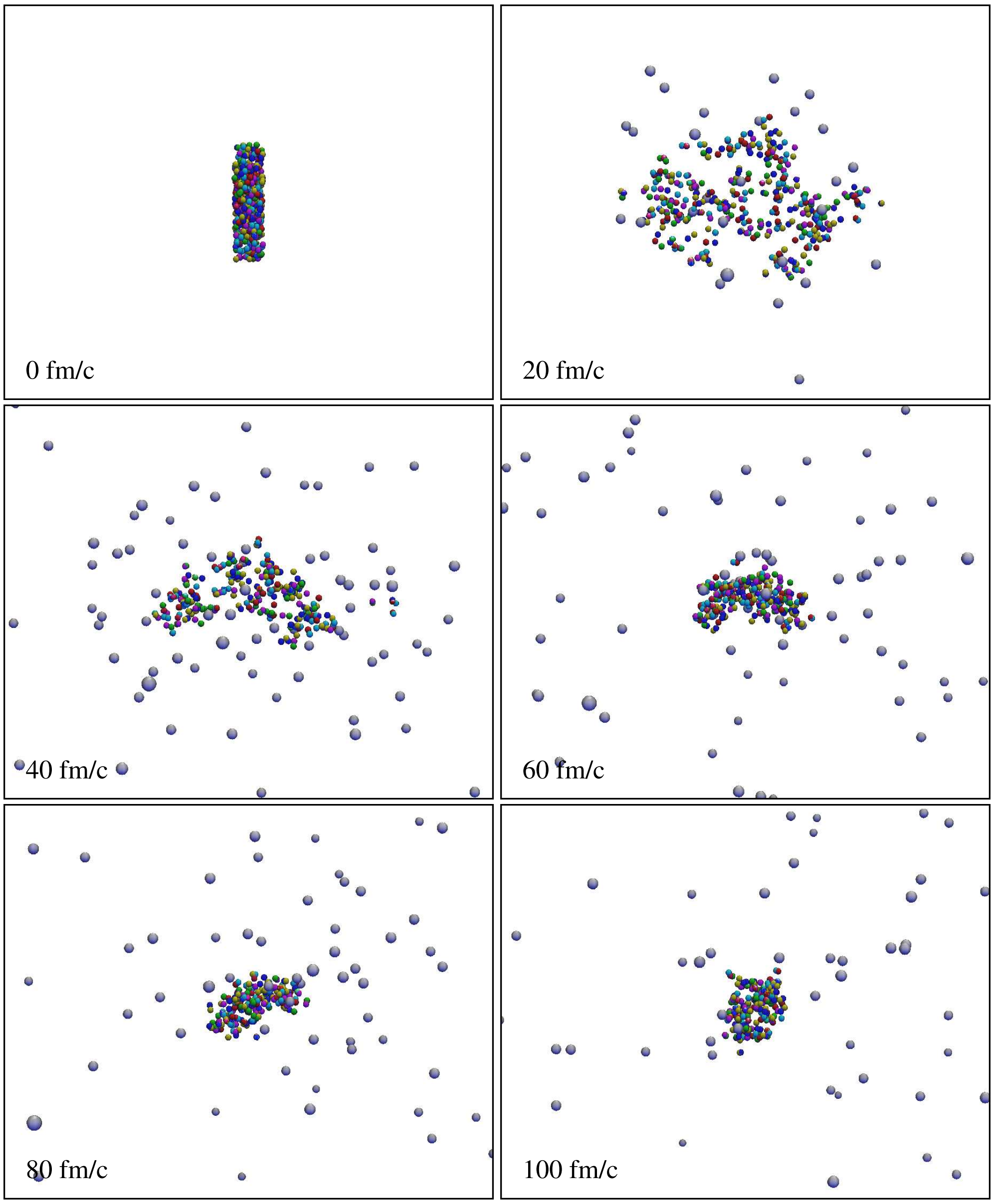

Fig. 9. Simulation snapshots after initialization of a central-rapidity slice of a QGP tube with Lorentz-invariant flow ("Bjorken scenario"). The frame diagonal is of length 45 fm. The labels at the particles and hadrons indicate the various flavors and constituents; the letter q represents an up or down quark; the other letters have obvious meanings, capital letters denoting antiquarks. Colored objects (quarks, gluons) are drawn in dark grey, hadrons in light grey.

as the two color fields are not displayed. Note that in the last frame, many hadrons have already left the scene.

As can be seen from the pictures, the initial partonic fireball is expanding and hadronizing. Whenever an irreducible white cluster is detected, it is classified according to Fig. 7.as a meson, baryon or glueball, its total energy, momentum and mass are computed, the partons and their field imprint are removed from the simulation and replaced by a noninteracting “hadron”, displayed in the snapshots as a grey sphere. We would like to emphasize that the production of hadronic states is not artificially put in by hand: the model itself produces irreducible white clusters in the final state, and it is only up to our detection routine to classify them and take them out of the simulation. The detection routine does not drive or interfere with the process of hadron formation, it merely serves to interpret the results. Although the last snapshot still shows quarks and gluons, this is not the final state of the simulation run. In the final state of the simulation run, hadronization is indeed complete: no partonic fireball is left over.

Fig. 10.shows for the same time interval the temperature evolution of the partons in the fireball and the produced hadrons. Their temperature is found from

$$\frac{3}{2}T \;:=\; \left\langle \frac{\vec{p}^{\,2}}{2m} \right\rangle . \tag{96}$$

The partons heat up initially because they are accelerated by relatively long (> 1 fm) flux tubes. These flux tubes are present simply because of the initial spatial random distribution of the charges. Very soon, however, the hot particles cool down, transferring energy to the σ field. On the same time scale, the energy contribution of the color electric field decreases to almost zero. This is an indication of the strong electric shielding of the plasma. The picture of the plasma as a collection of flux tubes breaks down here; flux tubes emerge only on the surface of the fireball, pulling back colored objects that try to escape. It is interesting to note that, although the energy contribution of the color field itself is never significant, the color field dictates the dynamics of the hadronization process, allowing only white objects to separate.

The hadronic energy contribution is a monotonous step function: it increases each time we take another quark-gluon cluster, delete its field imprint and add it to the set of hadrons in the system. The hadrons do no longer interact, hence the piecewise constant energy. About half of the final energy is deposited in σ waves. This energy has its origin in the initialized thermal energy of the color charges. These form flux tubes, and via the coupling term $\kappa(\sigma)F^2/4$ the flux tube cools down, radiating σ waves. The $\sigma-$field describes the long-range collective effects of QCD. Its large energy content shows that the nonperturbative QCD vacuum is highly excited; in the “real world”, it would decay mostly into pions which are so far not contained in our simulation.

Note that most of the final hadronic energy is produced in the time interval $[10\text{fm}, 50\text{fm}]$. These 40 fm could be interpreted as the hadronization time in our model.

There is no final-state interaction among the hadrons or between hadrons and partons in the simulation, so the hadronic subsystem is not in thermal contact with the fireball. This is realistic: the hadron temperature reflects the parton temperature at the time of hadron formation (freeze-out point). Since most of the hadrons are produced in the time interval $[10\text{fm}, 50\text{fm}]$, the final hadronic temperature reflects the fireball temperature at that time. The fireball cools further

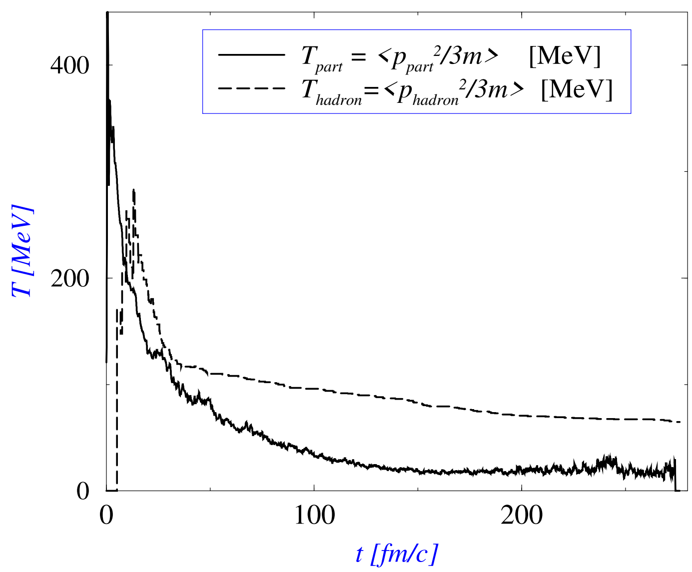

Fig. 10. Particle and hadron temperature over time in the Bjorken event.

down, which leads to the unrealistic picture that after about 50 fm, the fireball is significantly cooler than the hadrons.

In an experiment, a fireball as cold as $50 MeV$ would probably hadronize immediately. In our simulation, however, hadrons are only well-defined once they have clearly left the fireball and can be *detected* as a separate, irreducible white cluster. At this late stage of the simulation run, hadronization is a random evaporation process: inside the fireball, color fields are strongly shielded, which prevents stable white clusters to form. So an irreducible white cluster (hadron) can only form at the surface of the fireball, as soon as its constituents, floating around in the fireball nearly freely, happen to reach the surface with coalescent momenta. Thus it takes quite some time for a small, cold parton cluster to hadronize completely.

We attribute this partly to the missing repulsive interaction between the white clusters in our simulation [62]. In addition, it is well known from nuclear fragmentation studies that the mean field tends to prevent clusterization [70]. Thus, fluctuations of the color fields may be important for the final hadronization process.

The final mass distribution of the hadrons is shown in Fig. 11.for the Bjorken scenario. The spectrum starts at a mass of 800 MeV because this is the mass of the lightest hadron ($q\bar{q}$) in our model, and no quarks or gluons are left over in the final state.

Assuming a Hagedorn density of hadronic states [71],

$$\rho(m) \;\propto\; m^a e^{m/T_H}, \tag{97}$$

we expect in the nonrelativistic limit a measured mass distribution

$$\frac{dN}{dm} \quad \propto \quad \rho(m) \int d^3p \, e^{-(m+p^2/2m)/T}$$

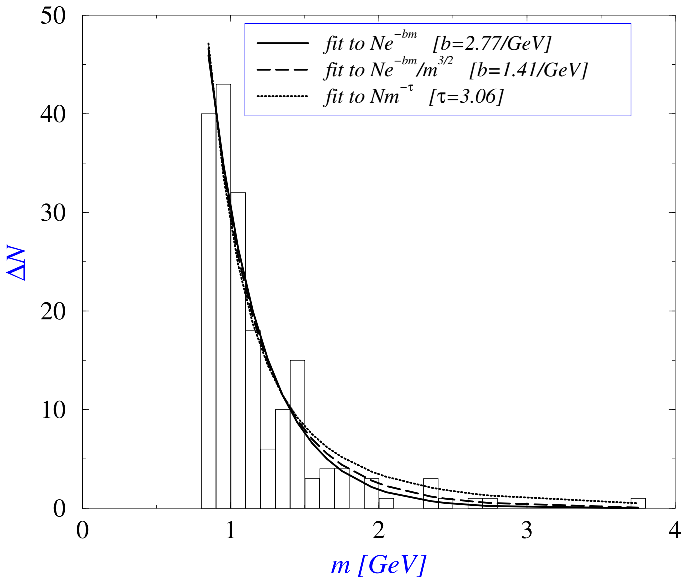

Fig. 11. Mass spectrum for the Bjorken case.

$$\propto \quad m^{a+\frac{3}{2}} e^{-m\left(\frac{1}{T}-\frac{1}{T_H}\right)}. \tag{98}$$

The nonrelativistic limit is justified by our large constituent masses. Here, T_H is the Hagedorn temperature: the limit temperature of hadronic strings. Beyond this temperature, the flux tube picture must be replaced by a true QGP. We assume $T_H = 160$ MeV for now (which is what Hagedorn estimated originally) and take $a = -3$ from [72]. Fig. 11.shows that a satisfactory fit of the form (98) can be obtained. Our fit parameter b is related to T via

$$b = \frac{1}{T} - \frac{1}{T_H}. \tag{99}$$

The corresponding hadron temperature is $T = 130$ MeV, which is somewhat higher than the kinetic temperature found in the last section. However, these numbers depend on the choice of a: taking $a = -3/2$, we expect a simple exponential curve for the mass spectrum, which results in a different value for T, namely $T = 110$ MeV. In this single-event analysis with our very small statistics, we cannot really decide on the correct value of a.

The hadron rapidity spectrum is approximately gaussian. No plateau structure is visible, since we have cut out a central-rapidity slice of the Bjorken tube. One could easily extrapolate this result by folding the rapidity spectrum with that of a Bjorken QGP tube of realistic extension. This folding process would then result in a plateau structure.

Fig. 12.shows the transverse momentum spectra of nonstrange white hadronic clusters observed in mass bins of width 0.6 GeV above 0.6 GeV. Although the points in the Figure representing mid-p_T values do not lie exactly on exponential curves, it is interesting to consider the slope values in order to extract possible information on the flow and temperature of the fireball

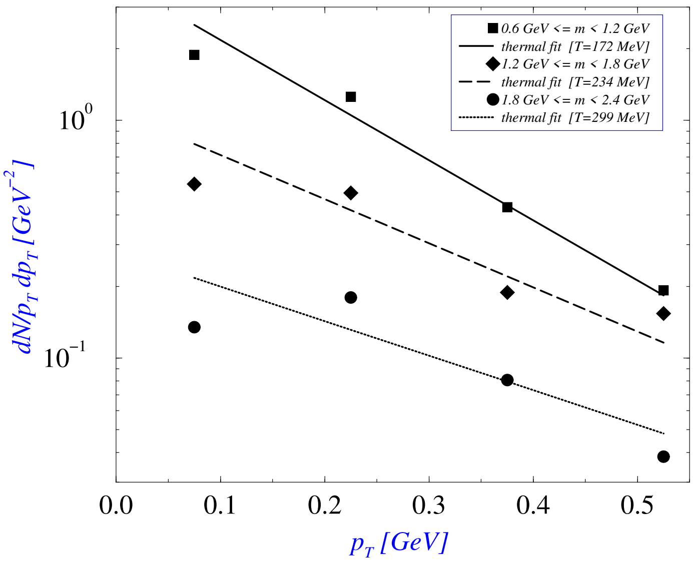

Fig. 12. Final transversal momentum spectrum for the Bjorken case, for three mass bins separately. When computing the fit lines, we took the statistical error bars correctly into account [64].

in the late hadronization phase. The resulting inverse slopes, denoted as "temperatures" $T(m)$, are displayed in Fig. 13.By fitting to the linear relation

$$T(m) = T_0 + m\langle v_T^2 \rangle, \tag{100}$$

we extract from the plot a temperature $T_0 = 77$ MeV and a radial flow $\sqrt{\langle v_T^2 \rangle} = 0.32$. A direct computation of the radial flow from our final state yields $\sqrt{\langle v_T^2 \rangle} = 0.30$, which is remarkably close. For the full stopping event, the same $T(m)$ analysis yields $T_0 = 126$ MeV and $\sqrt{\langle v_T^2 \rangle} = 0.18$, while the true radial flow is $\sqrt{\langle v_T^2 \rangle} = 0.27$, a not so good agreement. Compared to data on SPS heavy ion experiments at CERN [74] ($\langle v_T \rangle = 0.4$, $v_{\max} = 0.6$ and $T = 140$ MeV) our results display a little less flow and a colder hadronic fireball. It should be noted, however, that this analysis is based on a single event whose plasma volume is only a fraction of the experimental one. Also, we extracted the spectra of rather heavy hadronic clusters; their decay products (with lower mass) may have higher p_T-slopes leading altogether to a higher estimate of T_0. From this viewpoint, the qualitative agreement is satisfactory.

3.2 Summary

We have investigated the hadronization process of a quark-gluon droplet in the framework of a simplified equation of state assuming saturated string interaction, the transchemistry model and the chromodielectric model, using a classical molecular dynamic approach. Our quark masses were fitted to a constituent model of the vector meson octet and baryon decuplet states. We determined from the microscopic data of hadronization events the mass-, rapidity- and transverse momentum distributions.

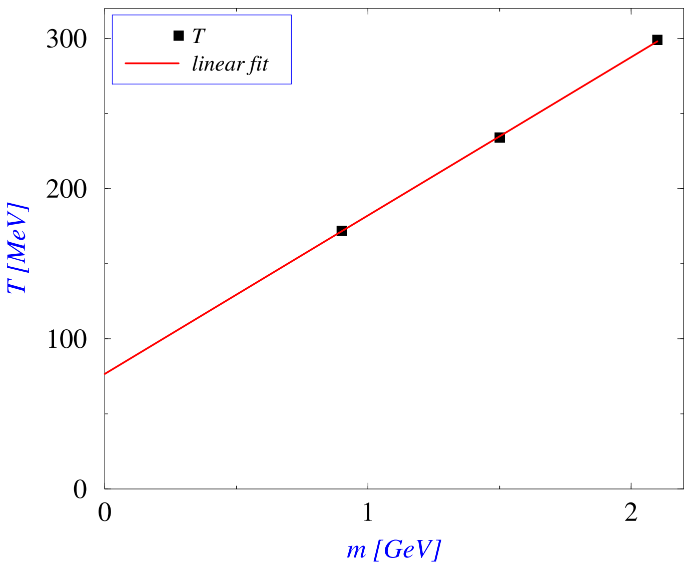

Fig. 13. The temperatures extracted from mass differential p_T spectra, plotted against hadron rest mass.

As an example we have taken an initial state, with one-dimensional scaling flow. We found that although the identification of white clusters technically requires a long simulation time, the mass distribution develops a hadron part already at the beginning of the process — about 10 fm after initialization — and the main hadronization process is done after another 25 fm have passed. In a recent RQMD paper [75] similar hadronization times are reported.

Hadronization is certainly a much faster process than this simulation suggests. This is because we can only uniquely identify an irreducible white cluster after it has already left the fireball. So in this simulation, hadronization looks like a slow evaporation effect, while in principle pre-hadrons could already form in the plasma but remain undetected by our program.

Summarizing, we do not observe a vast departure from thermal equilibrium during this microscopic study of hadronization. Chemical equilibration on the other hand is incomplete as shown by the deviation between the Maxwell-Boltzmann slopes for different cluster species and in general between colored and white particles. This also supports the conclusion that during the late hadronization of quark matter there is no phase equilibrium between the quark-gluon and hadron components; the Gibbs criteria do not apply. The suggested picture is rather a mixture of hadronic and quark-gluon plasma counterparts (with additive instead of equal pressure) as has been studied in all three models presented in these lectures.

Acknowledgements This work was supported by the Hungarian National Fund for Scientific Research (OTKA T019700, T024094), by American - Hungarian Joint Fund (MAKA JFNo 649) and by a common project of the Hungarian academy of Science and the Deutsche Forschungsgemeinschaft (DFG-MTA 101/1998). Stimulating discussions with B. Müller, S. G. Matinyan, J.Knoll, A.A.Shanenko and V.Toneev are acknowledged.

References

[1] G. Röpke, D. Blaschke, H. Schulz: *Phys. Rev.* **D34** (1986) 3499

[2] G. Röpke, D. Blaschke, H. Schulz: *Phys. Lett.* **B202** (1988) 479

[3] Ch. Barter, D. Blaschke, H. Voss: i*Phys. Lett.* **B293** (1992) 423

[4] L. Diósi, B. Lukács: *Phys. Lett.* **A112** (1985) 13

[5] L. Diósi, B.Lukács: *Phys. Rev.* **A31** (1985) 3415

[6] A. Einstein: *Annalen der Physik* **33** (1910) 1275

[7] T. S. Biró, J. Zimányi: *Phys. Lett.* **B113**(1982) 6; *Nucl. Phys.* **A395** (1983) 525

[8] P. Koch, B. Müller, J. Rafelski: *Phys. Rep.* **C142** (1986) 167

[9] H. W. Barz, B. L. Friman, J. Knoll, H. Schulz: *Nucl. Phys.* **A484** (1988) 661; **A519** (1988) 831; **A545** (1992) 259

[10] E. Braaten, R. D. Pisarski: *Phys. Rev.* **D42** (1990) 2156 ; **D45** (1992) 1827; **D46** (1992) 1829; *Nucl. Phys.* **B339** (1990) 310; for a recent review see: M. H. Thoma: *hep-ph/9801266*

[11] B. Kämpfer, O. P. Pavlenko, A. Peshier, G. Soff, *Proc. of Strangeness in Hadronic Matter*, Tucson, 1995, ed. J. Rafelski, AIP, 1995; A. Peshier, B. Kämpfer, O. P. Pavlenko, G. Soff: *Phys. Rev.* **D54** (1996) 2399

[12] P. Lévai and U. Heinz, Phys. Rev. C **57**, 1879 (1998).

[13] T. S. Biró, J. Zimányi, P. Lévai: *Phys. Lett.* **B347** (1995) 6

[14] T. S. Biró, P. Lévai, J. Zimányi: *Proc. of Strangeness in Hadronic Matter*, Tucson, 1995, ed. J. Rafelski, AIP, 1995; J. Zimányi, T. S. Biró, T. Csörgö, P. Lévai: *Heavy Ion Phys.* **4** (1996) 15

[15] P.Braun-Munzinger, J.Stachel, J.P.Wessels, N.Xu: *Phys.Lett.* **B365** (1996) 1

[16] I. Montvay, J. Zimányi: *Nucl. Phys.* **A316** (1979) 490

[17] J. D. Bjorken: *Phys. Rev.* **D27** (1983) 140

[18] T. Matsui, B. Svetitsky, L. McLerran: *Phys. Rev.* **D34** (1986) 783 ; Erratum **D37** (1988) 844; T. Matsui, B. Svetitsky: *Phys. Rev.* **D34** (1986) 2047

[19] J.Zimányi, P. Lévai, B.Lukács, A.Rácz: *in Particle Production in Highly Excited Matter,* Eds. H.H. Gutbrod and J. Rafelski, Plenum Press, New York, 1993

[20] L. P. Csernai, J. I. Kapusta: *Phys. Rev. Lett.* **69** (1992) 737; *Phys. Rev.* **D46** (1992) 1379 ; E. E. Zabrodin, L. P. Csernai, J. I. Kapusta, G. Kluge: *Nucl. Phys.* **A566** (1994) 407c

[21] E.G.Nikonov, A.A.Shanenko, V.Toneev: *nucl-th/9802018*

[22] J. Zimányi, T.S. Biró, P. Lévai: *J. Phys.* **G23** (1997) 1941

[23] Particle Data Group, Review of Particle Properties, *Phys. Rev.* **D50** (1994) 1173

[24] H. Sorge: *Phys. Rev.* **C52** (1995) 3291; *Nucl. Phys.* **A590** (1995) 571c

[25] S.V. Afanasiev *et al.*, NA49 Coll.: *Nucl. Phys.* **A610** (1996) 188c

[26] C. Bormann, for the NA49 Coll.: *J. Phys.* **G23** (1997) 1817

[27] S. Margetis, for the NA49 Coll.: *Heavy Ion Phys.* **4** (1996) 63

[28] A.K. Holme, for the WA97 Coll.: *J. Phys.* **G23** (1997) 1851

[29] I. Kralik *et al.*, WA97 Coll.: *Nucl. Phys.* **A638** (1998) 115c

[30] *We thank J. Knoll for calling attention to this fact.*

[31] H. Satz: *in Proc. of the Conference "Quark Matter 91"*, Gatlinburg, TN, USA, Nov 11-15, 1991, Nucl. Phys. A 544, 371, 1992.

[32] M. Creutz: *Quarks, gluons and lattices*, Cambridge University Press, Cambridge, 1983; for a recent review see: C. DeTar, in *Quark-Gluon Plasma 2*, ed. R. C. Hwa, World Scientific, Singapore, 1995, p. 1.

[33] E. Braaten, R. D. Pisarski: *Phys. Rev.* **D42** (1990) 2156; for a recent review see: M. H. Thoma: in *Quark-Gluon Plasma 2*, ed. R. C. Hwa, World Scientific, Singapore, 1995, p. 51.

[34] L. V. Keldysh: *Sov. Phys. JETP* **20** (1965) 1018

[35] *Proc. of the Workshop on "QCD at Finite Baryon Density"*, Bielefeld, April 27-30, 1998; W. Bietholz, U.-J. Wiese: i*hep-lat/9801022*; S. D. Hsu, M. Schwetz: *hep-ph/9803386*; R. Aloisio, V. Azcoiti, G. DiCarlo, A. Galante, A. F. Grillo: *hep-lat/9709118*, *hep-lat/9804020*; I. M. Barbour, S. E. Morrison, E. G. Klapfish, J. B. Kogut, M.-P. Lombardo: *hep-lat/9705042*; W. Bietenholz: *in Proc. of the Workshop on "QCD at Finite Baryon Density"*, Bielefeld, April 27-30, 1998, *hep-lat/9805014*

[36] B. Andersson, G. Gustafsson, G. Ingelman, T. Sjöstrad: *Phys. Rep.* **97** (1983) 33
B. Andersson, G. Gustafsson, B. Nielssen-Almquist: *Nucl. Phys.* **B281** (1987) 289

[37] H. Fukuda, C. Iso: *Prog. Theor. Phys.* **60** (1978) 1439; S. A. Azimov, G. M. Chernov, K. G. Gularnov, V. Sh. Navotnyi, N. S. Scripnik: *Phys. Lett.* **73** (1978) 500; D. H. Boal: *Phys. Rev.* **C33** (1986) 2206

[38] R. J. Glauber: *in Proc. of Methods in Subnuclear Physics*, Vol. V., part 1, pp 1-52, Herceg-novi 1969, New York, 1977; R. J. Glauber: *in Geometrical pictures in hadronic collisions*, p. 83, ed. S. Y. Lo, 1987.

[39] R. P. Feynman, R. D. Field: *Phys. Rev.* **D15** (1977) 2590; *Nucl. Phys.* **B136** (1978) 1

[40] K. Geiger, B. Müller: *Nucl. Phys.* **B369** (1992) 600; K. Geiger: *Phys. Rep.* **258** (1995) 238; J. Ellis, K. Geiger: *Phys. Rev.* **D54** (1996) 1755.

[41] K. Werner: *Z. Phys.* **C42** (1989) 85; *Phys. Rep.* **232** (1993) 87

[42] S. A. Bass, M. Belkacem, M. Bleicher, M. Brandstetter, L. Bravina, C. Ernst, L. Gerland, M. Hofmann, S. Hofmann, J. Konopka, G. Mao, L. Neise, S. Soff, C. Spieles, H. Weber, L. A. Winckelmann, H. Stocker, W. Greiner, C. Hartnack, J. Aichelin, N. Amelin: *Prog. Part. Nucl. Phys.* **41** (1998) 254
S. A. Bass *et al.*: *nucl-th/9804058*

[43] H. Sorge, H. Stöcker, W. Greiner: *Ann. Phys.* **192** (1989) 266

[44] T. S. Biró, P. Lévai, J. Zimányi: *Phys. Lett.* **B347** (1995) 6; *J. Phys.* **G23** (1997) 1941

[45] E. G. Nikonov, A. A. Shanenko, V. D. Toneev: *nucl-th/9802018; private communication*

[46] H. W. Barz, B. L. Friman, J. Knoll, H. Schulz: *Nucl. Phys.* **A484** (1988) 661

[47] T. S. Biró, P. Lévai, J. Zimányi: *hep-ph/9807303*

[48] P. Rehberg, S. P. Klevansky, J. Hüfner: *Phys. Rev.* **C53** (1996) 410; P. Rehberg, S. P. Klevansky, J. Hüfner: *Nucl. Phys.* **A608** (1996) 356; S. P. Klevansky, P. Rehberg, A. Ogura, J. Hüfner: *in Proc. of Workshop on QCD Phase Transitions*, Hirschegg 1997, p 397, Ed. H. Feldmeier, J. Knoll, *hep-ph/9701355*

[49] R. Friedberg, T. D. Lee: *Phys. Rev.* **D15** (1977) 1694; *Phys. Rev.* **D16** (1977) 1096

[50] R. Goldflam, L. Wilets: *Phys. Rev.* **D25** (1982) 1951; L. Wilets: in *Chiral Solitons*, ed. K.F.Liu, World Scientific, Singapore, 1987; G. Fái, R. J. Perry, L. Wilets: *Phys. Lett.* **B208** (1988) 1

[51] S. Kahana, G. Ripka: *Nucl. Phys.* **A429** (1984) 462

[52] U. Mosel: *Fields, Symmetries and Quarks*, McGraw-Hill, London, 1989.

[53] U. Kalmbach, T. Vetter, T. S. Biró, U. Mosel: *Nucl. Phys.* **A563** (1993) 584

[54] T. Vetter, T. S. Biró, U. Mosel: *Nucl. Phys.* **A581** (1995) 598

[55] T. Vetter: *Ph. D. Thesis* Giessen 1994.

[56] S. Loh, T. S. Biró, U. Mosel, M. H. Thoma: *Phys. Lett.* **B387** (1996) 685

[57] S. Loh: *Ph. D. Thesis*x, Giessen 1997.

[58] T. Elze, U. Heinz: *Phys. Rep.* **183** (1989) 81

[59] E. Naar, M. C. Birse: *J. Phys.* **G19** (1993) 555

[60] J. A. McGovern, M. C. Birse, D. Spanos: *J. Phys.* **G16** (1990) 1561

[61] L. Wilets: *Nontopological Solitons*, World Scientific, Singapore, 1989

[62] W. Koepf, L. Wilets, S. Pepin, F. Stancu: *Phys. Rev.* **C50** (1994) 614; W. Koepf, L. Wilets: *Phys. Rev.* **C51** (1995) 3445

[63] L. Wilets, R. D. Puff: *Phys. Rev.* **C51** (1995) 339

[64] W. H. Press, S. A. Teukolsky, W. T. Vetterling, B. P. Flannery: *Numerical Recipes in C*, 2nd Edition, Cambridge 1992.

[65] R. E. Bank, T. F. Dupont, H. Yserentant: *Num. Math.* **52** (1988) 427

[66] C. T. Traxler: *Computing 59* (1997) 115

[67] W. Mitchell: *SIAM J. Sci. Stat. Comp.* **13** (1992) 146

[68] D. H. Perkins: *Introduction to High Energy Physics*, Addison-Wesley 1987.

[69] H.Satz: i*hep-ph/9805418*

[70] C. Jung, W. Cassing, U. Mosel: *Nucl. Phys.* **A477** (1988) 256

[71] R. Hagedorn: *Nuovo Cim. Suppl.* **3** (1965) 147; G. Veneziano: *Nuovo Cim.* **57A** (1968) 190

[72] M. I. Gorenstein, V. A. Miransky, V. P. Shelest, G. M. Zinovjev, H. Satz: *Nucl. Phys.* **B76** (1974) 453

[73] D. Stauffer: *Phys. Rep.* **54** (1978) 1; D. Stauffer, A. Aharony: *Introduction to Percolation Theory*, London 1992

[74] N. Xu (NA44 Collaboration): *Nucl. Phys.* **610A** (1996) 175c

[75] H. van Hecke, H. Sorge, N. Xu: *nucl-th/9804035*